Targeted Foxe1 overexpression in mouse thyroid causes the development of multinodular goiter but does not promote carcinogenesis

Alyaksandr Nikitski[1,9], Vladimir Saenko[2], Mika Shimamura[3], Masahiro Nakashima[4], Michiko Matsuse[1], Keiji Suzuki[1], Tatiana Rogounovitch[5], Tetiana Bogdanova[6], Nobuyuki Shibusawa[7], Masanobu Yamada[7], Yuji Nagayama[3], Shunichi Yamashita[1,2], and Norisato Mitsutake[1,8]

[1]Department of Radiation Medical Sciences, Atomic Bomb Disease Institute, Nagasaki University, 1-12-4 Sakamoto, Nagasaki 852-8523, Japan;

[2]Department of Radiation Molecular Epidemiology, Atomic Bomb Disease Institute, Nagasaki University, 1-12-4 Sakamoto, Nagasaki 852-8523, Japan;

[3]Department of Molecular Medicine, Atomic Bomb Disease Institute, Nagasaki University, 1-12-4 Sakamoto, Nagasaki 852-8523, Japan;

[4]Department of Tumor and Diagnostic Pathology, Nagasaki University, 1-12-4 Sakamoto, Nagasaki 852-8523, Japan;

[5]Department of Global Health, Medicine and Welfare; Atomic Bomb Disease Institute, Nagasaki University, 1-12-4 Sakamoto, Nagasaki 852-8523, Japan;

[6]Laboratory of Morphology of Endocrine System, State Institution 'V.P. Komisarenko Institute of Endocrinology and Metabolism of Academy of Medical Sciences of Ukraine', Vishegorodskaya Street 69, Kyiv 254114, Ukraine

[7]Department of Medicine and Molecular Science, Gunma University Graduate School of Medicine, 3-39-15 Showa-machi, Maebashi, Gunma 371-8511, Japan

[8]Nagasaki University Research Centre for Genomic Instability and Carcinogenesis (NRGIC), 1-12-4 Sakamoto, Nagasaki 852-8523, Japan.

[9]Nagasaki University Graduate School of Biomedical Sciences, 1-12-4 Sakamoto, Nagasaki 852-8523, Japan.

Abbreviated title: Tg-Foxe1 mice induces multinodular goiter

Key terms: Foxe1, thyroid, transgenic mouse, mouse model, multinodular goiter

Word count: 4678

Number of figures and tables: 7

Corresponding author and person to whom reprint should be addressed:

Norisato Mitsutake, MD PhD

Department of Radiation Medical Sciences, Atomic Bomb Disease Institute, Nagasaki University

1-12-4 Sakamoto, Nagasaki 852-8523, Japan

Tel.: +81-95–819-7116

Fax: +81-95–819-7117

E-mail: mitsu@nagasaki-u.ac.jp

Disclosure statement: The authors have nothing to disclose.

Abstract

Recent genome-wide association studies have identified several single nucleotide polymorphisms in the *FOXE1* locus, which are strongly associated with the risk for thyroid cancer. In addition, our recent work has demonstrated FOXE1 overexpression in papillary thyroid carcinomas. To assess possible contribution of Foxe1 to thyroid carcinogenesis, transgenic mice overexpressing Foxe1 in their thyroids under thyroglobulin promoter (*Tg-Foxe1*) were generated. Additionally, *Tg-Foxe1* mice were exposed to X-rays at the age of 5 weeks or crossed with $Pten^{+/-}$ mice to examine the combined effect of Foxe1 overexpression with radiation or activated PI3K-Akt pathway, respectively. In 5–8 weeks old *Tg-Foxe1* mice, severe hypothyroidism was observed, and mouse thyroids exhibited hypoplasia of the parenchyma. Adult 48-week-old mice were almost recovered from hypothyroidism, their thyroids were enlarged and featured colloid microcysts and multiple benign nodules of macrofollicular-papilloid growth pattern, but no malignancy was found. Exposure of transgenic mice to 1 Gy or 8 Gy of X-rays and *Pten* haploinsufficiency promoted hyperplastic nodule formation also without carcinogenic effect. These results indicate that Foxe1 overexpression is not directly involved in the development of thyroid cancer, and that proper Foxe1 dosage is essential for achieving normal structure and function of the thyroid.

Introduction

FOXE1 is a thyroid-specific forkhead transcription factor crucial for craniopharyngeal embryogenesis and for the maintenance of differentiated state of thyroid. Germline loss-of-function *FOXE1* mutations in humans are the basis for the rare autosomal-recessive Bamforth-Lazarus syndrome characterized by cleft palate, spiky hair, choanal atresia, bifid epiglottis and congenital hypothyroidism due to thyroid dysgenesis (1). Foxe1 deficiency in mice also leads to developmental abnormalities such as thyroid ectopy or loss of thyroid follicular cell (TFC) progenitors. Interestingly, the initiation of thyroid primordium formation at early stages of embryogenesis and functional differentiation of the TFC precursors are not impaired in Foxe1-null mice (2).

In functionally differentiated human TFC, FOXE1 regulates several thyroid-specific genes such as *TG*, *TPO*, *NIS* and *DUOX2* (3-4), acting as a classical pioneer transcription factor (5-6). FOXE1 is a useful marker of differentiated state of normal or neoplastic thyroid tissues, and its expression correlates with differentiation level of thyroid cancer cells. Previous studies showed that FOXE1 expression is significantly down-regulated in poorly differentiated thyroid carcinoma and is absent in anaplastic thyroid cancer (7-8). On the other hand, our recent work has demonstrated FOXE1 overexpression and cytoplasmic translocation in human papillary thyroid carcinoma (PTC) (9). FOXE1 expression is not only elevated in PTC but also correlates with some clinicopathological features such as extra-capsular invasion, tumor stage and lymph node metastasis (10). Moreover, recent genome-wide and target gene association studies have identified two single-nucleotide polymorphisms (SNPs), rs965513 located 60 kb upstream of *FOXE1* and rs1867277 in the 5'UTR of the same gene, which confer risk for thyroid cancer (11-12). These SNPs may be involved in transcriptional regulation of *FOXE1*. For instance, the risk allele of rs1867277 (A) enhances the activation of *FOXE1* promoter in Hela cells through the recruitment of UCF transcription factors (13). Nevertheless, the precise role of FOXE1 in thyroid tumorigenesis is not fully understood so far.

To assess possible contribution of Foxe1 to thyroid carcinogenesis, we generated transgenic mice overexpressing Foxe1 under thyroglobulin promoter (*Tg-Foxe1*). Additionally, *Tg-Foxe1* mice

were exposed to X-rays at the age of 5 weeks or crossed with $Pten^{+/-}$ mice to address the combined effect of Foxe1 overexpression with radiation or activated PI3K-Akt pathway, respectively. Surprisingly, we found that *Tg-Foxe1* mice developed thyroid hypoplasia and overt hypothyroidism shortly after birth, but at older age had multinodular goiter. Congenital hypothyroidism (CH) is observed in 1:2000 to 1:4000 of neonates (14-15). The vast majority (up to 85%) of primary CH cases are caused by thyroid dysgenesis associated with loss-of-function mutations in *TSHR, PAX8, NKX2-1, FOXE1* and *NKX2-5*, while dyshormonogenesis accounts for 10-15% of cases due to mutations in *SLC5A5*, *TPO*, *DUOX2*, *DUOXA2*, *SLC26A4*, *TG* and *IYD/DEHAL1* (16-17). It should be noted that follicular (18-22) and papillary thyroid carcinoma (23-26) may arise from dyshormonogenetic goiter. No data on FOXE1 overexpression in CH or its effect on either human or murine thyroid is available, and comprehensive understanding of CH with subsequent goiter or thyroid carcinogenesis is impeded by the lack of adequate animal models.

Here we introduce the first mouse model of thyroid-specific overexpression of Foxe1 and provide a detailed histopathological characterization of Foxe1-associated hypothyroidism followed by the development of multinodular goiter. The combined effect of Foxe1 overexpression with X-ray irradiation or activated PI3K-Akt pathway is also presented.

Materials and Methods

Mice

A mouse model of targeted expression of Foxe1 driven by the bovine thyroglobulin promoter was generated. Fragment of the bovine thyroglobulin promoter (2045 bp), the murine *Foxe1* gene (1116 bp) and the SV-40 polyadenylation signal (228 bp) were cloned into the pBlue-script-II SK+ vector (Stratagene, CA, USA). For transgenesis, purified construct DNA was microinjected into zygotes and transferred into pseudopregnant C57BL/6J females at the UNITECH facility (Chiba,

Japan). Transgene integration into the genome of founders was confirmed by Southern blotting. Two independent lines were established. Founder mice were mated with wild-type C57BL/6J partners, and the progeny was screened for the presence of transgene by PCR as described below. Heterozygous *Pten*-knockout mice (B6.129-*Pten*<tm1Rps>, hereafter designated as *Pten*$^{+/-}$ mice) were obtained from National Cancer Institute at Frederick, USA. Double transgenic mice were obtained by cross-mating of *Tg-Foxe1* mice with *Pten*$^{+/-}$ mice.

Mice were bred in a specific pathogen-free facility and fed with a standardized regular diet. Animal care and all experimental procedures were performed in accordance with the Guidelines for Animal Experimentation of Nagasaki University with the approval of the Institutional Animal Care and Use Committee.

PCR genotyping

Genotyping was performed at the age of 4 weeks by PCR using tail-extracted DNA (REDExtract-N-Amp Tissue PCR KIT; Sigma, USA) or amnion-derived DNA for embryos. The primers used to detect the *Tg-Foxe1* transgene were: 5'-CTACAGCCTCCACAAGATTTTCA-3' and 5'-TGAGTTTGGACAAACCACAACTA-3' yielding a 1552-bp PCR product. The primers for *Pten*$^{+/-}$ mice were: P012 (5'-TTGCACAGTATCCTTTTGAAG-3') and P013 (5'-GTCTCTGGTCCTTACTTCC-3') yielding a 240-bp product for wild-type *Pten*; and P012 and P014 (5'-ACGAGACTAGTGAGACGTGC -3') yielding a 320-bp product for *Pten*.

X-ray irradiation

Wild-type and *Tg-Foxe1* littermates were exposed to 1 Gy or 8 Gy of X-rays at the age of 5 weeks. Mice were anesthetized by intraperitoneal injection of Nembutal (Sodium Pentobarbital) into the lower left quadrant of abdomen at a dose of 40 mg/kg and immobilized. Unshielded front neck area was exposed to X-rays at a dose rate of 0.5531 Gy/min using a Toshiba ISOVOLT TITAN 320.

Animal groups, and tissue and serum sampling

In the present study, mice were divided into four main groups according to the genetic background: C57BL/6J wild-type mice (WT), *Tg-Foxe1*, *Pten*$^{+/-}$ and double transgenic *Tg-Foxe1/Pten*$^{+/-}$. Not exposed to X-ray WT and *Tg-Foxe1* mice were subdivided into four age groups: 5–8, 24–48 weeks; mice exposed to X-ray were sacrificed at the age of 8, 24 and 48 weeks. *Pten*$^{+/-}$ and *Tg-Foxe1/Pten*$^{+/-}$ mice were examined at the age of 5–8 and 24 weeks.

At the indicated time points, mice were anesthetized by intraperitoneal injection of Nembutal at the dose of 50 mg/kg. Blood was collected by cardiac puncture, and the animals were euthanized by cervical dislocation. Thyroid lobes were dissected and weighted. One lobe was snap-frozen in liquid nitrogen and stored at -80°C until use, and the other was put in 10% neutral-buffered formalin. After 24 h fixation in formalin at 4°C, tissue samples were rinsed in water and embedded into paraffin. Five-micrometer-thick serial sections were prepared for further hematoxylin-eosin or immunohistochemical staining. For cryosectioning, fresh tissue samples were washed in ice-cold PBS and frozen in Tissue-Tek O.C.T. compound (Sakura Finetek, USA). Sections were taken in a cryostat Leica CM3050 S (Leica Biosystems).

Brown adipose tissue staining

Cryosections were fixed in 10% formalin for 15 min at 4°C. After intensive washing in distilled water, slides were incubated in propylene glycol 2 x 5 min and stained with 150 nM solution of Sudan Black B in propylene glycol for 7 min with agitation. After washing for 3 min in 85% propylene glycol and rinsing in distilled water, sections were counterstained with Nuclear Fast Red (Sigma, USA) for 5 min and mounted with aqueous mounting media.

Immunohistochemistry (IHC)

Formalin-fixed paraffin-embedded (FFPE) 4 μm serial sections were deparaffinized and subjected to antigen retrieval in a microwave in Tris-EDTA buffer, pH 9.0 at 95°C for 25 min (for Foxe1 antigen unmasking) or in citrate buffer, pH 6.0 at 95°C for 25 min (for Ttf-1, Thyroglobulin, Calcitonin and Ki-67 antigens unmasking). Blocking reagent (Dako, Denmark) was applied at room temperature (RT) for 1 hr. After blocking, the sections were incubated with primary antibodies diluted in Antibody Diluent (Dako, Denmark) solution: rabbit anti-TTF1 (1:750; Biopat, Italy), rabbit anti-TTF2 (1:750; Biopat, Italy), rabbit anti-Thyroglobulin (1:1000; Dako, Denmark), rat anti-Ki67 (1:100; Dako, Denmark), rabbit anti-PTEN (1:400; Abcam, UK) and anti-Calcitonin (prediluted; Dako, USA) overnight at 4°C. After washing, HRP-conjugated secondary antibodies anti-Rabbit (1:100, Dako, Denmark) or anti-Rat (1:100, Dako, Denmark) were applied for 1 hour at RT. Detailed information about antibodies used in this study is presented in Supplemental Table 1. Visualization was performed with DAB Enhanced Liquid Substrate System tetrahydrocloride (Sigma, USA). Nuclei were counterstained with hematoxylin.

The intensity score of nuclear Foxe1 staining was categorized as negative (0), weak (1), mild (2) or strong (3). The proportion score was determined as a percentage of positively stained nuclei of thyroid epithelial cells within the intensity category. The total Foxe1 immunohistochemistry score (IHC-score) was calculated as a sum of products of staining intensity scores and corresponding proportion scores. Ki-67 labeling index was calculated as a percentage of positively stained nuclei of thyroid epithelial cells. At least 1000 thyroid epithelial cells were counted in 5 random fields at ×400 magnification for evaluation of the Foxe1 IHC-score and Ki-67 labeling index.

Dual-labeled immunofluorescence analysis

Formalin-fixed paraffin-embedded (FFPE) 4 μm sections were deparaffinized and subjected to antigen retrieval in a microwave in Tris-EDTA buffer, pH 9.0 at 95°C for 20 min. Sections were

blocked for 1 hour in 5% BSA in PBS, and incubated with primary antibodies diluted in 5% skim milk in TBST: rabbit anti-TTF2 (1:250; Biopat, Italy) and rat anti-Ki67 (1:50; Dako, Denmark) overnight at 4°C. Sections were then incubated with 4', 6-diamidino-2-phenolindole (1:1000; DAPI; Dojindo, Japan) and secondary antibodies diluted in 5% skim milk in TBST: anti-rabbit Alexa Fluor 546 and anti-rat Alexa Fluor 647 (1:1000, Invitrogen, USA) for 1 hour at RT. Stained slides were imaged using a BZ-9000 microscope (Keyence, Osaka, Japan) and were recorded with a BZ-II analysis application (Keyence). Exposition time for 450 nm, 546 nm and 647 signals were optimized to obtain the widest dynamic range of recorded fluorescence intensity.

Quantitative real-time reverse transcription-PCR (qRT-PCR)

Total RNA was extracted from homogenized fresh-frozen thyroid tissues with ISOGEN reagent (Nippon Gene, Tokyo, Japan). Two hundred nanograms of total RNA were transcribed with ReverTra Ace qPCR RT Master Mix with gDNA Remover (Toyobo, Japan). Quantitative PCR was carried out in a Thermal Cycler Dice Real-time system (Takara Bio Inc., Otsu, Shiga, Japan) using SYBR Premix Ex Taq II reagent (Takara Bio Inc., Otsu, Shiga, Japan). The profile of thermal cycle was as follows: 95ºC for 2 min, 40 cycles of 95ºC for 5 sec and 60ºC for 30 sec, followed by dissociation curve analysis for all primer pairs. The average of the relative quantity of replicates was calculated with Q-Gene software (27) using *Actb* (β-actin) or *Pax8* data for normalization. Sequences of the primers are listed in Supplemental Table 2.

Serum Free T4, T3 and TSH measurement

FT4 and FT3 were measured using standard laboratory assay (SRL Inc.). Mouse serum TSH was measured using in-house radioimmunoassay as described previously (28).

Statistical analysis

Statistical comparison of categorical variables was performed using the 3x2 or 4x2 extensions of Fisher's exact test (http://in-silico.net/tools/statistics/fisher_exact_test/2x3). Continuous data were analyzed by applying non-parametrical Mann-Whitney *U*-test for comparison of two groups or Kruskal-Wallis test for multiple group comparisons as appropriate. Analysis was performed with IBM SPSS Statistics Version 21 and GraphPad 4.1 Prism (GraphPad Software) software packages. All p-values were 2-sided and considered significant if <0.05.

Results

Generation of *Tg-Foxe1* mice

For thyroid-specific overexpression of Foxe1, a 3.4 kb genetic construct combining the bovine thyroglobulin promoter, the murine *Foxe1* and the SV-40 polyadenylation signal was created (Figure 1A). Two independent founder lines bearing 12 (line A) and 2 (line B) copies of the transgene were established. Both lines developed similar thyroid phenotype within 48 weeks of life span (Supplemental Figure 1A). Transgenic *Foxe1* expression was verified by qRT-PCR with transgene-specific primers (Supplemental Figure 1B). The line A bearing a greater number of transgene copies was chosen for the detailed investigation.

qRT-PCR assessment of transgenic *Foxe1* expression demonstrated its age-dependent decline (Figure 1B). Total *Foxe1* expression (i.e., endogenous and transgenic *Foxe1* combined) did not change with age in wild-type (WT) mice but was decreasing in *Tg-Foxe1* animals (Figure 1C). By the age of 48 weeks no difference in total *Foxe1* expression was observed between transgenic and WT animals. The decrease in total *Foxe1* expression in *Tg-Foxe1* mice with age is thus likely to be fully attributed to the decline in the expression of the *Foxe1* transgene.

Foxe1 overexpression in the thyroids of *Tg-Foxe1* mice was confirmed by IHC (Figure 1D). The proportion of cells showing the highest score (3, "strong") of immunoreactivity to Foxe1 remained significantly higher in *Tg-Foxe1* mice compared to WT at all age groups (Figure 1E), but the drastic difference at 5–8 weeks declined at 24–48 weeks. Similar observations were made for the total Foxe1 IHC score (Figure 1F). The results of IHC corresponded well with qRT-PCR data.

Systemic characterization of the *Tg-Foxe1* mice

No obvious differences between newborn *Tg-Foxe1* mice and their WT siblings were observed. However, the signs of growth retardation became apparent 2–3 weeks after birth. The *Tg-Foxe1* mice exhibited cretinous body habitus (Figure 2A) and significantly lower body weight in both males and females until the age of 8 weeks (Figure 2B). The thyroid weights of 5- and 8-week-old *Tg-Foxe1* mice were comparable to those of WT mice, but became significantly greater at 24 and 48 weeks (Figure 2C). The thyroid-weight-to-body-weight ratio was significantly higher in *Tg-Foxe1* than in WT mice at 8, 24 and 48 weeks, but not at 5 weeks (Figure 2D). Gross anatomy of transgenic animals was normal except thyroid. As representatively shown for the 48-week-old mice (Figure 2E), *Tg-Foxe1* animals had enlarged thyroids with irregular surface and visible nodules.

Taking into consideration the essential role of Foxe1 in thyroid primordium migration and TFC precursors survival, mouse embryos were examined histologically. Thyroid bud formation and migration of TFC precursors towards the front neck area was not altered. The thyroid reached its conventional position at E14.5. The appearance of isolated TFC highly positive for Foxe1 in E14.5 transgenic mice (Supplemental Figure 2A) coincided with the onset of thyroglobulin expression (29). The ultimobranchial bodies were successfully enclosed by thyroid tissue. As a result, widely disseminated calcitonin-positive cells were detected in the thyroids of postnatal transgenic animals (Supplemental Figure 2B).

Tg-Foxe1 mice developed hypothyroidism

Because of the pronounced growth retardation in transgenic mice, serum TSH, FT4 and FT3 were measured. TSH levels were significantly elevated and FT4 diminished in 5 and 8 weeks old *Tg-Foxe1* mice (Figure 3). Despite there was no difference in TSH levels between *Tg-Foxe1* and WT mice in 24–48-week-old animals, serum FT4 was gradually increased but not fully recovered. We also measured serum FT3 in *Tg-Foxe1* and WT mice, and surprisingly they were not different in all age group (Figure 3). We therefore examined the expression of *Dio1* (type I deiodinase) and *Dio2* (type II deiodinase) in the extracted thyroid lobes. Both *Dio1* and *Dio2* expression in *Tg-Foxe1* mice were robustly up-regulated in young animals and then declined but still remained higher than in WT mice even at the older age (Supplemental Figure 3), which may be the reason for imbalance between FT4 and FT3.

We also measured transcriptional levels of thyroid-specific genes *Slc5a5* (*Nis*, sodium/iodide symporter), *Tpo* (thyroid peroxidase), *Duox2* (dual oxidase 2) and *Slc26a4* (*Pds*, Pendrin), which could be regulated by Foxe1 and are involved in thyroid hormone biosynthesis. Compared to WT mice, all except *Duox2* were age-dependently up-regulated, presumably due to corresponding Foxe1 overexpression, but none was suppressed (Supplemental Figure 3). Therefore, hypothyroidism in young *Tg-Foxe1* mice was not caused by the disruption of thyroid hormone biosynthesis and was mainly due to thyroid hypoplasia (see histological description below). On the whole, our observations indicate that *Tg-Foxe1* mice exhibited severe hypothyroidism in young age and a gradual recovery until 48 weeks.

Histological features of the thyroid in young (5–8 weeks old) mice

At the age of 5–8 weeks, thyroids of WT animals showed predominantly normo-microfollicular structure without pathological abnormalities. In contrast, thyroids of *Tg-Foxe1* mice displayed the abnormal irregular architecture with dominant micro-normofollicular, minor macrofollicular, solid and papilloid areas (Figures 4, A and B). Thyroid epithelium in the papilloid

areas showed some oxyphilic changes. The number of thyroid follicles in the young transgenic animals was decreased in comparison to the control littermates; normal parenchyma was abundantly substituted by brown adipose tissue (BAT) (Figure 4A) as confirmed by staining of thyroid cryosections with Sudan Black B and qRT-PCR for *Ucp1* (Supplemental Figures 4A and B). In some animals, BAT occupied more than 40% of the thyroid volume (Supplemental Figure 4C). In *Tg-Foxe1* mice, thyroid follicles were predominantly filled with pale colloid; some follicles contained heterogeneous, foamed or depleted colloid (Figure 4B, b).

Thyroid follicles in WT mice were predominantly lined by a single uniform layer of cuboidal epithelium and a small fraction of flattened epithelial cells at the periphery of the gland. Besides of conventional epithelium, thyroids of *Tg-Foxe1* mice featured tall cuboidal and columnar follicular cells (Figure 4B, b). Thyrocytes of young Foxe1 overexpressing mice also displayed prominent nuclear pleomorphism and hyperchromatosis, especially in solid clusters; giant hyperchromatic/bizarre nuclei were also revealed.

Functional differentiation of thyroid follicular cells was confirmed by IHC for thyroglobulin, Ttf-1 and Foxe1 (Figure 5A). Interestingly, some thyrocytes in transgenic animals showed stronger cytoplasmic thyroglobulin staining than in control mice. The intensity and proportion of Ttf-1 staining was similar between *Tg-Foxe1* and WT littermates. The intensity of Foxe1 immunoreactivity was heterogeneous in thyrocytes in both transgenic and WT mice. Nevertheless, the total Foxe1 IHC-score was significantly higher in 5–8 weeks old transgenic mice in comparison to WT animals (see also Figure 1F). Small immature follicles contained thyrocytes with the highest intensity of Foxe1 staining were commonly seen (Figure 5A, arrow in the Foxe1 panel), while in mature follicles and areas of focal hyperplasia such cells were less frequent.

In transgenic mice, tall cuboidal and columnar thyrocytes had eosinophilic cytoplasm likely due to a high level of TSH stimulation. Concordantly, a proliferative index estimated by Ki-67 IHC (Figure 5B) was significantly higher as compared to that in WT animals both in 5–8-week old males and females (Figure 6A). Histologically, the high level of follicular cell proliferation activity was

represented by numerous papilloid structures inside follicular lumens and initial signs of hyperplastic nodule formation (as was demonstrated in Figures 4A and B). Interestingly, Ki-67-positive follicular cells had moderate to low levels of Foxe1 (Figure 5C), strongly suggesting that cells overexpressing Foxe1 were unlikely to be involved in the active proliferation upon TSH stimulation.

Histological features of the thyroid in mature/adult (24–48 weeks old) mice

The thyroids of WT mice at 24–48 weeks displayed normo-macrofollicular structure with normal age-associated histopathological changes. In transgenic mice, from the age of 24 weeks, hyperplastic areas of diffuse macrofollicular structure and hyperplastic micronodules were observed. The number of cells with nuclear pleomorphism and hyperchromatosis were drastically decreased in adult *Tg-Foxe1* mice in comparison to 5–8-week-old ones. Marked accumulation of the colloid resulted in dilatation of follicles and formation of colloid microcysts. (Figure 4C and D). Gradual decrease of BAT content was also noted (Supplemental Figure 4C).

At 24–48 weeks, follicular epithelium of WT mice was predominantly cuboid and, to a less extent, flattened. In *Tg-Foxe1* mice, macrofollicular thyroid structures contained somewhat flattened cuboid or fully flattened cells (Figure 4D, a). At the age of 48 weeks, well-formed hyperplastic, predominantly macrofollicular-papilloid micronodules in transgenic mice were seen (Figure 4D). Enlarged follicles contained papilloid projections of cuboid or columnar eosinophilic cells with pleomorphic nuclei (Figure 4D, b). Hyperplastic papilloid micronodules in *Tg-Foxe1* mice did not show any specific features of papillary thyroid carcinoma such as capsular/lymphovascular invasion or nuclear grooves, pseudo-inclusions and optical clearing. Small hyperplastic follicles protruding into the lumen of larger follicles, so called Sanderson's pollsters, were also found.

At the age of 24–48 weeks, transgenic mice, both males and females, showed lower Ki-67 labeling indexes compared to 5–8 weeks old mice. Nevertheless, it remained significantly higher as compared to that in WT animals (Figure 6). Thus, by the age of 48 weeks *Tg-Foxe1* mice did not

develop thyroid cancer, but the gland was affected by a diffuse macrofollicular hyperplastic process with multiple macro-normo-papilloid hyperplastic micronodules and colloid microcysts.

Effect of X-ray exposure

Irradiation of thyroids of WT mice with 1 Gy or 8 Gy of X-rays at the age of 5 weeks resulted in prominently flattened follicular epithelium and dilatation of the follicular lumen at the age of 48 weeks in comparison to non-exposed mice (Figure 7A). Exposure of *Tg-Foxe1* mice significantly promoted hyperplastic micronodule formation (Figure 7B). After exposure to 1Gy, well-formed hyperplastic micronodules were found from 8 weeks of age, and from 24 weeks after 8 Gy. Despite the delay in micronodule formation (as compared to 1 Gy exposure), a significantly higher frequency of micronodules was observed in the latter group at 48 weeks of age ($p<0.01$). Histopathological features of thyroid micronodules in exposed *Tg-Foxe1* animals were similar to those in unexposed transgenic mice of the same age. Thus, exposure of Foxe1-overexpressing animals to ionizing radiation stimulated the formation of hyperplastic nodules in a dose-related manner without carcinogenic effect.

Double transgenic *Tg-Foxe1/Pten*$^{+/-}$ mice

Double transgenic *Tg-Foxe1/Pten*$^{+/-}$ animals developed severe hypothyroidism at the age of 5 weeks similarly to *Tg-Foxe1* mice. Congenital hypothyroidism was characterized by significant growth retardation, significantly elevated serum TSH and diminished FT4 (data not shown). Thyroid follicular epithelium was profoundly substituted by BAT. Colloid in normo-, micro- and macrofollicles was heterogeneous: pale, depleted, foamed and sometimes with mucinous content. Cellular areas showing pleomorphism of follicular cells with nuclear enlargement and hyperchromasia were observed.

Activation of the follicular epithelium in 5–8 weeks old *Tg-Foxe1/Pten*$^{+/-}$ mice was observed: cuboidal thyrocytes had increased eosinophilic cytoplasm with small clear vacuoles. Hyperplastic changes such as papilloid projections into the follicular lumen, nuclear crowding and foci of columnar cells, were more frequent in 5–8-week-old double transgenic mice in comparison to age-matched *Tg-Foxe1* and *Pten*$^{+/-}$ mice. The proliferation rate of thyroid epithelial cells in *Tg-Foxe1/Pten*$^{+/-}$ mice was significantly higher in comparison to *Pten*$^{+/-}$ animals at 5 and 8 weeks of age (Figure 6). Immunohistochemical staining showed that there was no loss of the remaining *Pten* allele in any age group (Supplemental Figure 5). Ki-67 labeling indexes did not differ significantly between *Tg-Foxe1/Pten*$^{+/-}$ and *Tg-Foxe1* mice in all age groups (Figure 6), indicating that heterozygous *Pten* deletion added a minor effect on the proliferative phenotype of *Tg-Foxe1* mice thyroids. On the other hand, the labeling indexes in *Tg-Foxe1/Pten*$^{+/-}$ and *Tg-Foxe1* mice were significantly higher than in age-matched WT animals (Figure 6).

In contrast to *Tg-Foxe1* and *Pten*$^{+/-}$ mice, double transgenic animals developed multiple hyperplastic thyroid micronodules from the age of 8 weeks (Figure 7 C and D). The frequency of micronodules in *Tg-Foxe1/Pten*$^{+/-}$ mice was significantly higher in comparison to *Pten*$^{+/-}$ animals. Note that *Pten*$^{+/-}$ mice had predominantly adenomatous nodules with normo-microfollicular-solid or normofollicular-solid structure, prominent oxyphilic changes of follicular cells and areas of nuclear pleomorphism. Micronodules in double transgenic mice showed mixed features of hyperplastic nodules found in *Tg-Foxe1* mice and adenomatous nodules of *Pten*$^{+/-}$ animals (Figure 7C). Thus, Foxe1 overexpression in thyroids of *Pten*$^{+/-}$ mice caused acceleration of hyperplastic processes, showing features of both *Pten*$^{+/-}$ and *Tg-Foxe1* phenotypes, but no cancerous nodules were seen.

Discussion

To evaluate the role of high level of Foxe1 as a possible etiological factor in thyroid carcinogenesis, transgenic mice overexpressing *Foxe1* under the thyroglobulin promoter were

generated. The transgenic animals were viable and showed no apparent gross developmental abnormalities. However, in the postnatal period, *Tg-Foxe1* mice at the age 5–8 weeks displayed congenital hypothyroidism manifesting as significant growth retardation, diminished level of FT4 and elevated TSH. In those mice, normal follicular organization in the thyroid gland was compromised, and thyroid parenchyma was replaced with BAT to a large extent.

Under the TSH stimulation, tall cuboidal and columnar thyrocytes with augmented eosinophilic cytoplasm appeared in the thyroids of transgenic mice. TSH-induced enhancement of thyroid hormone synthesis was accompanied by the activation of endocytosis in thyrocytes seen as colloid depletion in some follicles. High TSH levels also switched on the growth of thyroid parenchyma. The thyroids of 5-week-old transgenic mice showed a high (>10%) Ki-67 labeling index. It is worth noting, however, that follicular cells overexpressing Foxe1 were unlikely to be the primary responders to TSH stimulation. Several facts concordantly support this notion: 1) in the areas of evident proliferation, the majority of cells displayed moderate levels of Foxe1 on IHC or immunofluorescence; 2) the proportion of cells with strong Foxe1 staining intensity was declining with the increase of thyroid weight; 3) small immature follicles highly immunoreactive for Foxe1 persisted in the thyroids of 5–8-week-old *Tg-Foxe1* mice; and 4) no Ki-67 signals were seen in the cells overexpressing Foxe1. It is likely that Foxe1 overexpression may prevent the proliferative cellular reaction on TSH stimulation. Under this scenario, thyroid parenchyma regeneration and hyperplastic changes seen in older mice would be achieved through the propagation of epithelial cells with lower Foxe1 level. The inability of cells with high Foxe1 levels to proliferate is also consistent with and may explain thyroid hypoplasia observed during the first month of postnatal life of *Tg-Foxe1* mice. Molecular mechanisms of interference between the proliferative signals and Foxe1 overexpression as well as age-dependent down-regulation of transgene expression require further investigation.

TSH-induced activation and proliferation of follicular cells led to the gradual increase of FT4 level. However, surprisingly, the FT3 level in the *Tg-Foxe1* mice was not different from WT mice in all age groups. This may be due to the increased level of *Dio1* and *Dio2* in the thyroids of the

transgenic animals. *Dio1* and *Dio2* were highly up-regulated in the 5–8-week-old *Tg-Foxe1* mice, in which BAT occupied a large part of thyroid tissue. It should be mentioned that TSH receptors are expressed in BAT cells and TSH stimulates *Dio2* expression in these cells (30).

Exposure of *Tg-Foxe1* mice thyroids to 1 Gy or 8 Gy of X-rays at the age of 5 weeks accelerated hyperplastic nodule formation in a dose-dependent manner. The changes were observed from 8-24 weeks of age, while irradiated WT mice did not develop any thyroid lesions. We speculate that high TSH may promote metaplastic changes in the thyroid follicular epithelium exposed to X-ray irradiation. A similar effect of TSH could be proposed with regard to Foxe1 overexpression combined with the activated PI3-Akt pathway. We found that hypothyroid 5 weeks old *Tg-Foxe1/Pten*$^{+/-}$ mice exhibited a remarkable increase in the thyrocyte proliferation rate as compared to age-matched *Pten*$^{+/-}$ mice. Moreover, double transgenic mice displayed an accelerated formation of hyperplastic and adenomatous nodules detectable from the age of 8 weeks, whose development was not due to the loss of the remaining *Pten* allele. More detailed investigation is needed to establish exact pathogenetic and molecular basis of these hyperplastic and neoplastic processes.

The model described in our study has some limitations. The overexpression of Foxe1 caused hypothyroidism, thus corresponding TSH elevation in young mice, and the transgene expression was then declined with age. This created a complicated situation, which made it difficult to asses the effect of Foxe1 overexpression only (i.e., without the hormone imbalance) on thyroid tumorigenesis. On the other hand, all transgenic mice displayed thyroid-related phenotype, and therefore the model may be useful for *in vivo* studies of the mechanisms of TSH-dependent proliferation of the thyrocytes or BAT cells under the condition of CH, and of pathogenesis of multinodular goiter.

In summary, our mouse model of thyroid-specific overexpression of Foxe1 allowed us to make several important observations. By the age of 5 weeks, transgenic mice displayed thyroid hypoplasia accompanied by the extensive replacement of thyroid parenchyma with BAT and the development of overt hypothyroidism. Likely due to the prolonged TSH stimulation at young age, the reactive proliferation of TFC took place and resulted in the nearly full compensation of

hypothyroidism by the age of 24 weeks and the development of hyperplastic changes representative of multinodular goiter. No direct evidence of thyroid carcinogenesis due to Foxe1 overexpression during the course of 48 week-long observation was found either in *Tg-Foxe1* mice, *Tg-Foxe1* mice exposed to 1–8 Gy of X-rays or in 24-week-old *Tg-Foxe1/Pten*$^{+/-}$ mice. We conclude that proper Foxe1 dosage is essential for thyroid development and functioning, and excessive Foxe1 in the thyroid does not induce carcinogenesis in our model.

Acknowledgments

This work was supported in part by Grants-in-Aid for Scientific Research 26293142 (to N.M.) and 26293222 (to S.Y.) from the Japan Society for the Promotion of Science.

References

1. Bamforth JS, Hughes IA, Lazarus JH, Weaver CM, Harper PS. Congenital hypothyroidism, spiky hair, and cleft palate. J Med Genet 1989; 26:49-51.

2. De Felice M, Ovitt C, Biffali E, Rodriguez-Mallon A, Arra C, Anastassiadis K, Macchia PE, Mattei MG, Mariano A, Scholer H, Macchia V, Di Lauro R. A mouse model for hereditary thyroid dysgenesis and cleft palate. Nat Genet 1998; 19:395-398.

3. Sinclair AJ, Lonigro R, Civitareale D, Ghibelli L, Di Lauro R. The tissue-specific expression of the thyroglobulin gene requires interaction between thyroid-specific and ubiquitous factors. Eur J Biochem 1990; 193:311-318.

4. Fernandez LP, Lopez-Marquez A, Martinez AM, Gomez-Lopez G, Santisteban P. New insights into FoxE1 functions: identification of direct FoxE1 targets in thyroid cells. PLoS One 2013; 8:e62849.

462 **5.** Cuesta I, Zaret KS, Santisteban P. The forkhead factor FoxE1 binds to the thyroperoxidase
463 promoter during thyroid cell differentiation and modifies compacted chromatin structure. Mol
464 Cell Biol 2007; 27:7302-7314.
465 **6.** Zaret KS, Carroll JS. Pioneer transcription factors: establishing competence for gene
466 expression. Genes Dev 2011; 25:2227-2241.
467 **7.** Nonaka D, Tang Y, Chiriboga L, Rivera M, Ghossein R. Diagnostic utility of thyroid
468 transcription factors Pax8 and TTF-2 (FoxE1) in thyroid epithelial neoplasms. Mod Pathol
469 2008; 21:192-200.
470 **8.** Sequeira MJ, Morgan JM, Fuhrer D, Wheeler MH, Jasani B, Ludgate M. Thyroid
471 transcription factor-2 gene expression in benign and malignant thyroid lesions. Thyroid 2001;
472 11:995-1001.
473 **9.** Bychkov A, Saenko V, Nakashima M, Mitsutake N, Rogounovitch T, Nikitski A, Orim F,
474 Yamashita S. Patterns of FOXE1 expression in papillary thyroid carcinoma by
475 immunohistochemistry. Thyroid 2013; 23:817-828.
476 **10.** Fan Y, Ding Z, Yang Z, Deng X, Kang J, Wu B, Zheng Q. Expression and clinical
477 significance of FOXE1 in papillary thyroid carcinoma. Mol Med Rep 2013; 8:123-127.
478 **11.** Gudmundsson J, Sulem P, Gudbjartsson DF, Jonasson JG, Sigurdsson A, Bergthorsson JT,
479 He H, Blondal T, Geller F, Jakobsdottir M, Magnusdottir DN, Matthiasdottir S, Stacey SN,
480 Skarphedinsson OB, Helgadottir H, Li W, Nagy R, Aguillo E, Faure E, Prats E, Saez B,
481 Martinez M, Eyjolfsson GI, Bjornsdottir US, Holm H, Kristjansson K, Frigge ML,
482 Kristvinsson H, Gulcher JR, Jonsson T, Rafnar T, Hjartarsson H, Mayordomo JI, de la
483 Chapelle A, Hrafnkelsson J, Thorsteinsdottir U, Kong A, Stefansson K. Common variants on
484 9q22.33 and 14q13.3 predispose to thyroid cancer in European populations. Nat Genet 2009;
485 41:460-464.
486 **12.** Takahashi M, Saenko VA, Rogounovitch TI, Kawaguchi T, Drozd VM, Takigawa-Imamura
487 H, Akulevich NM, Ratanajaraya C, Mitsutake N, Takamura N, Danilova LI, Lushchik ML,
488 Demidchik YE, Heath S, Yamada R, Lathrop M, Matsuda F, Yamashita S. The FOXE1 locus

is a major genetic determinant for radiation-related thyroid carcinoma in Chernobyl. Hum Mol Genet 2010; 19:2516-2523.

13. Landa I, Ruiz-Llorente S, Montero-Conde C, Inglada-Perez L, Schiavi F, Leskela S, Pita G, Milne R, Maravall J, Ramos I, Andia V, Rodriguez-Poyo P, Jara-Albarran A, Meoro A, del Peso C, Arribas L, Iglesias P, Caballero J, Serrano J, Pico A, Pomares F, Gimenez G, Lopez-Mondejar P, Castello R, Merante-Boschin I, Pelizzo MR, Mauricio D, Opocher G, Rodriguez-Antona C, Gonzalez-Neira A, Matias-Guiu X, Santisteban P, Robledo M. The variant rs1867277 in FOXE1 gene confers thyroid cancer susceptibility through the recruitment of USF1/USF2 transcription factors. PLoS Genet 2009; 5:e1000637.

14. Toublanc JE. Comparison of epidemiological data on congenital hypothyroidism in Europe with those of other parts in the world. Horm Res 1992; 38:230-235.

15. Harris KB, Pass KA. Increase in congenital hypothyroidism in New York State and in the United States. Mol Genet Metab 2007; 91:268-277.

16. Brown RS, Demmer LA. The etiology of thyroid dysgenesis-still an enigma after all these years. J Clin Endocrinol Metab 2002; 87:4069-4071.

17. Szinnai G. Clinical genetics of congenital hypothyroidism. Endocr Dev 2014; 26:60-78.

18. Cooper DS, Axelrod L, DeGroot LJ, Vickery AL, Jr., Maloof F. Congenital goiter and the development of metastatic follicular carcinoma with evidence for a leak of nonhormonal iodide: clinical, pathological, kinetic, and biochemical studies and a review of the literature. J Clin Endocrinol Metab 1981; 52:294-306.

19. Camargo R, Limbert E, Gillam M, Henriques MM, Fernandes C, Catarino AL, Soares J, Alves VA, Kopp P, Medeiros-Neto G. Aggressive metastatic follicular thyroid carcinoma with anaplastic transformation arising from a long-standing goiter in a patient with Pendred's syndrome. Thyroid 2001; 11:981-988.

20. Alzahrani AS, Baitei EY, Zou M, Shi Y. Clinical case seminar: metastatic follicular thyroid carcinoma arising from congenital goiter as a result of a novel splice donor site mutation in the thyroglobulin gene. J Clin Endocrinol Metab 2006; 91:740-746.

21. Hishinuma A, Fukata S, Kakudo K, Murata Y, Ieiri T. High incidence of thyroid cancer in long-standing goiters with thyroglobulin mutations. Thyroid 2005; 15:1079-1084.

22. Medeiros-Neto G, Gil-Da-Costa MJ, Santos CL, Medina AM, Silva JC, Tsou RM, Sobrinho-Simoes M. Metastatic thyroid carcinoma arising from congenital goiter due to mutation in the thyroperoxidase gene. J Clin Endocrinol Metab 1998; 83:4162-4166.

23. Yashiro T, Ito K, Akiba M, Kanaji Y, Obara T, Fujimoto Y, Hirayama A, Nakajima H. Papillary carcinoma of the thyroid arising from dyshormonogenetic goiter. Endocrinol Jpn 1987; 34:955-964.

24. Raef H, Al-Rijjal R, Al-Shehri S, Zou M, Al-Mana H, Baitei EY, Parhar RS, Al-Mohanna FA, Shi Y. Biallelic p.R2223H mutation in the thyroglobulin gene causes thyroglobulin retention and severe hypothyroidism with subsequent development of thyroid carcinoma. J Clin Endocrinol Metab 2010; 95:1000-1006.

25. Drut R, Moreno A. Papillary carcinoma of the thyroid developed in congenital dyshormonogenetic hypothyroidism without goiter: Diagnosis by FNAB. Diagn Cytopathol 2009; 37:707-709.

26. Kallel R, Mnif Hachicha L, Mnif M, Hammami B, Ayadi L, Bahri I, Ghorbel A, Abid M, Makni S, Boudawara T. [Papillary carcinoma arising from dyshormonogenetic goiter]. Ann Endocrinol (Paris) 2009; 70:485-488.

27. Muller PY, Janovjak H, Miserez AR, Dobbie Z. Processing of gene expression data generated by quantitative real-time RT-PCR. Biotechniques 2002; 32:1372-1374, 1376, 1378-1379.

28. Shibusawa N, Yamada M, Hirato J, Monden T, Satoh T, Mori M. Requirement of thyrotropin-releasing hormone for the postnatal functions of pituitary thyrotrophs: ontogeny study of congenital tertiary hypothyroidism in mice. Mol Endocrinol 2000; 14:137-146.

29. Milenkovic M, De Deken X, Jin L, De Felice M, Di Lauro R, Dumont JE, Corvilain B, Miot F. Duox expression and related H2O2 measurement in mouse thyroid: onset in embryonic development and regulation by TSH in adult. J Endocrinol 2007; 192:615-626.

30. Murakami M, Kamiya Y, Morimura T, Araki O, Imamura M, Ogiwara T, Mizuma H, Mori M. Thyrotropin receptors in brown adipose tissue: thyrotropin stimulates type II iodothyronine

deiodinase and uncoupling protein-1 in brown adipocytes. Endocrinology 2001; 142:1195-1201.

Figure legends

Figure 1. Generation and analysis of *Tg-Foxe1* mice. A, The genetic construct used to generate the *Tg-Foxe1* mice. The bovine thyroglobulin promoter (bTg, 2045 bp), murine *Foxe1* gene (*Foxe1*, 1116 bp) and the SV-40 polyadenylation signal (pA, 228 bp) are indicated by the rectangles. For Southern blotting, the 2770 bp Sph I/BamH I restriction fragment was hybridized with a probe located in the bTg area. For PCR screening of the *Foxe1* transgene, primers were designed to amplify the 1552 bp region spanning the bTg and pA sequences. B, Relative cDNA levels of transgenic *Foxe1* in the thyroid of *Tg-Foxe1* line A determined by qRT-PCR and normalized for *Pax8* expression. For qRT-PCR assessment of transgenic *Foxe1* expression, primers located in the 3' end of *Foxe1* and in pA sequences were used. Data are presented as a mean±SE of triplicates averaged for 8 mice for each group. C, Relative cDNA levels of total *Foxe1* in the thyroids of WT and *Tg-Foxe1* line A determined by qRT-PCR and normalized for *Pax8* expression. For qRT-PCR assessment of *Foxe1* expression, primers located in the coding region of *Foxe1* were used. Data are presented as a mean±SE of triplicates averaged for ~~3~~ 8 mice for each group. D, Representative images of thyroid histology and Foxe1 immunoreactivity in WT and *Tg-Foxe1* mice of different age. H&E and IHC for Foxe1. E and F, The proportion of cells with the highest intensity score (3, "strong") in Foxe1 IHC. F, The total Foxe1 IHC score. In E and F, the boxes include 50% of the values; lines inside the boxes represent median values; whiskers indicate the 10–90% range; *p<0.01, **p<0.001, ***p<0.0001.

Figure 2. Systemic characterization of *Tg-Foxe1* mice. A, Body habitus of representative female WT and *Tg-Foxe1* mice at the age of 5 weeks. B, Body weight (males n=7–24 mice/group, females n=8–

38 mice/group); C, Thyroid weight (males n=5–16 mice/group, females n=8–38 mice/group) and D, Thyroid-to-body-weight ratio (males n=5–16 mice/group, females n=8–38 mice/group) in WT and *Tg-Foxe1* animals of different age. Boxes include 50% of the values; lines inside the boxes represent median values; whiskers indicate the 10–90% range; **p*<0.01, ***p*<0.001, ***p<0.0001. E, Gross anatomy of WT and *Tg-Foxe1* mouse thyroids at the age of 48 weeks. Arrow points at the irregular surface of the thyroid.

Figure 3. The hypothyroid status of *Tg-Foxe1* mice. A, C and E, Relative TSH (A), FT4 (C) and FT3 (E) levels in WT and *Tg-Foxe1* mice of different age. The median value is represented by the solid line. Horizontal dashed lines represent the first (Q1) and the third quartile (Q3) of the relative TSH or FT4 values in WT mice estimated for each sex separately (see below). TSH (B), FT4 (D) and FT3 (F) level category in WT (n=6–11 mice/group) and *Tg-Foxe1* (n=6–9 mice/group) animals of different age combined for both sexes (see below).

Because of limitations in the in-house produced reagent availability and small sample volumes, statistical analysis of raw TSH, FT4 and FT3 concentrations in separate subgroups of male and female animals was impeded. We therefore determined the normal ranges of relative sex-specific TSH and FT4 levels as intervals between the first (Q1) and the third (Q3) quartiles calculated from the integrated data across all age groups of WT mice (distributions between which did not differ significantly, p>0.05, Kruskal-Wallis test). The defined normal ranges of relative TSH level in WT mice were 0.85–1.06 ng/ml (n=15) and 0.52–0.78 ng/ml (n=14) for males and females, respectively; 0.70–0.92 ng/dL (n=17) and 0.63–1.02 ng/dL (n=16) for FT4; and 1.16–1.38 pg/mL (n=23) and 1.18–1.35 pg/mL (n=24) for FT3. Then each raw value was categorized as diminished (<Q1), normal (Q1-Q3) or elevated (>Q3) for either TSH, FT4 or FT3. This approach allowed merging data for two sexes to increase statistical power. Differences between WT (n=6-11 mice/group) and *Tg-Foxe1* (n=6–11 mice/group) animals were evaluated using the 3x2 Fisher's exact test extension.

596 **Figure 4.** Histopathology of the *Tg-Foxe1* thyroid at different age. A, Representative
597 microphotographs of *Tg-Foxe1* and WT mice thyroids at the age of 5 weeks, H&E staining. BAT
598 denotes brown adipose tissue, arrows point at foci of hyperplastic micronodules. B, The representative
599 image of 8-week-old *Tg-Foxe1* thyroid with a colloid microcyst (Mc) and featuring (a) abnormal
600 solid/papilloid structures, and (b) colloid heterogeneity and columnar follicular epithelium (arrow). C,
601 The representative image of 24-week-old *Tg-Foxe1* thyroid. D, The representative image of 48-week-
602 old *Tg-Foxe1* thyroid; (a) area with flattened thyroid epithelium and (b) a nodule with papilloid
603 structures.
604
605 **Figure 5.** Functional differentiation and proliferative status of thyroid cells in young *Tg-Foxe1* and
606 *WT* mice. A, H&E and IHC for thyroglobulin, Ttf-1 and Foxe1, serial sections. The arrow in the
607 Foxe1 panel indicates immature follicle with high Foxe1 level. B, IHC for Ki-67. C, Double
608 immunofluorescent staining for Ki-67 (green) and Foxe1 (red). Nuclei were counterstained with DAPI.
609 PS, papillary structures.
610
611 **Figure 6.** Ki-67 labeling index in the thyroids of mice of different age. A, *Tg-Foxe1* (n=5–16
612 mice/group), $Pten^{+/-}$ (n=5–8 mice/group) and *Tg-Foxe1/*$Pten^{+/-}$ (n=5–9 mice/group) males. B, *Tg-*
613 *Foxe1* (n=8–12 mice/group), $Pten^{+/-}$ (n=7–9 mice/group) and *Tg-Foxe1/*$Pten^{+/-}$ (n=4–11 mice/group)
614 females. Boxes include 50% of the values; lines inside the boxes represent median values; whiskers
615 indicate the 10-90% range; *p<0.05, **p<0.01, ***p<0.001.
616
617 **Figure 7.** Combination effect of Foxe1 overexpression with X-ray irradiation or activated PI3K-Akt
618 signaling pathway. A, Representative microphotographs showing X-ray-associated histopathological
619 changes in WT and *Tg-Foxe1* mice thyroids at the age of 48 weeks, H&E staining. Scale bar, 0.5mm,
620 applies to all microphotographs. B, Frequencies of micronodule finding in thyroids of *Tg-Foxe1* mice
621 of different age by X-ray dose. Differences between unexposed (n=14–28 mice/group), and exposed
622 to 1 Gy (n=12–14 mice/group) or 8 Gy (n=13–14 mice/group) of X-rays mice were evaluated using

the 3x2 Fisher's exact test extension: *p<0.01, **p<0.001, ***p<0.0001; ns: not significant. C, Representative images of histopathological features of thyroids in 24 weeks old *Tg-Foxe1/Pten*$^{+/-}$ and *Pten*$^{+/-}$ mice, H&E staining. Hyperplastic areas with adenomatous (Ad) and papillary (Pap) structures. D, Frequencies of micronodules in thyroids of *Tg-Foxe1/Pten*$^{+/-}$ (n=14–21 mice/group) and *Pten*$^{+/-}$ (n=15–17 mice/group) mice of different age, *p<0.01.

Supplemental Figure 1. A, Histological structure of thyroids from two *Tg-Foxe1* lines A and B at the age of 48 weeks showing diffuse goiter with micronodules, H&E staining. B, Relative cDNA levels of transgenic *Foxe1* in the thyroids of two *Tg-Foxe1* lines determined by qRT-PCR and normalized for *Actb* (β-actin) expression. Data are presented as a mean±SE of triplicates for 3 mice in each group.

Supplemental Figure 2. Normal thyroid development in *Tg-Foxe1* mice. A, Representative microphotographs of the thyroid of *Tg-Foxe1* and WT mice at E14.5, H&E and IHC staining. Ts: thymus, Th: thyroid, UB: ultimobranchial body. B, Representative images of *Tg-Foxe1* thyroid lobe at the age of 5 weeks, frontal plane, H&E and IHC for Thyroglobulin, calcitonin (Ct) and Ttf-1, serial sections.

Supplemental Figure 3. Real-time PCR analysis of the relative expression of thyroid hormone biosynthesis-related *Dio1* and *Dio2* genes normalized for *Actb* (β-actin) or Pax8, and of *Slc5a5* (*Nis*), *Tpo*, *Duox2* and *Slc26a4* (*Pendrin*) normalized for *Pax8*, and relative expression of *Pax8* and *Ucp1* normalized for *Actb*. Data are presented as a mean±SE of duplicates for 8 mice in each group.

Supplemental Figure 4. Brown adipose tissue (BAT) in *Tg-Foxe1* and WT mice. A, Prominent BAT accumulation in the thyroid of a 8-week-old *Tg-Foxe1* mouse in comparison to an age- and sex-

matched WT animal. Cryosections were stained with H&E or Sudan Black B, nuclei counterstained with Nuclear Fast Red. B, Relative *Ucp1* expression in the thyroids of 8-week-old WT and *Tg-Foxe1* mice determined by qRT-PCR and normalized for *Actb* (β-actin). Data are presented as a mean±SE of triplicates (n=3 mice/group). BAT from the interscapular region of WT mice was used as a positive control (WT BAT). C, Relative amount of BAT in the thyroids of *Tg-Foxe1* and WT mice of different age. Differences between *Tg-Foxe1* (n=14–28 mice/group) and WT (n=13–19 mice/group) animals were evaluated using the 4x2 Fisher's exact test extension, ***$p<0.0001$.

Supplemental Figure 5. Representative images of IHC for Pten in 24-week-old mice of different genetic backgrounds. Similar results were obtained for animals of any age.

Figure 1

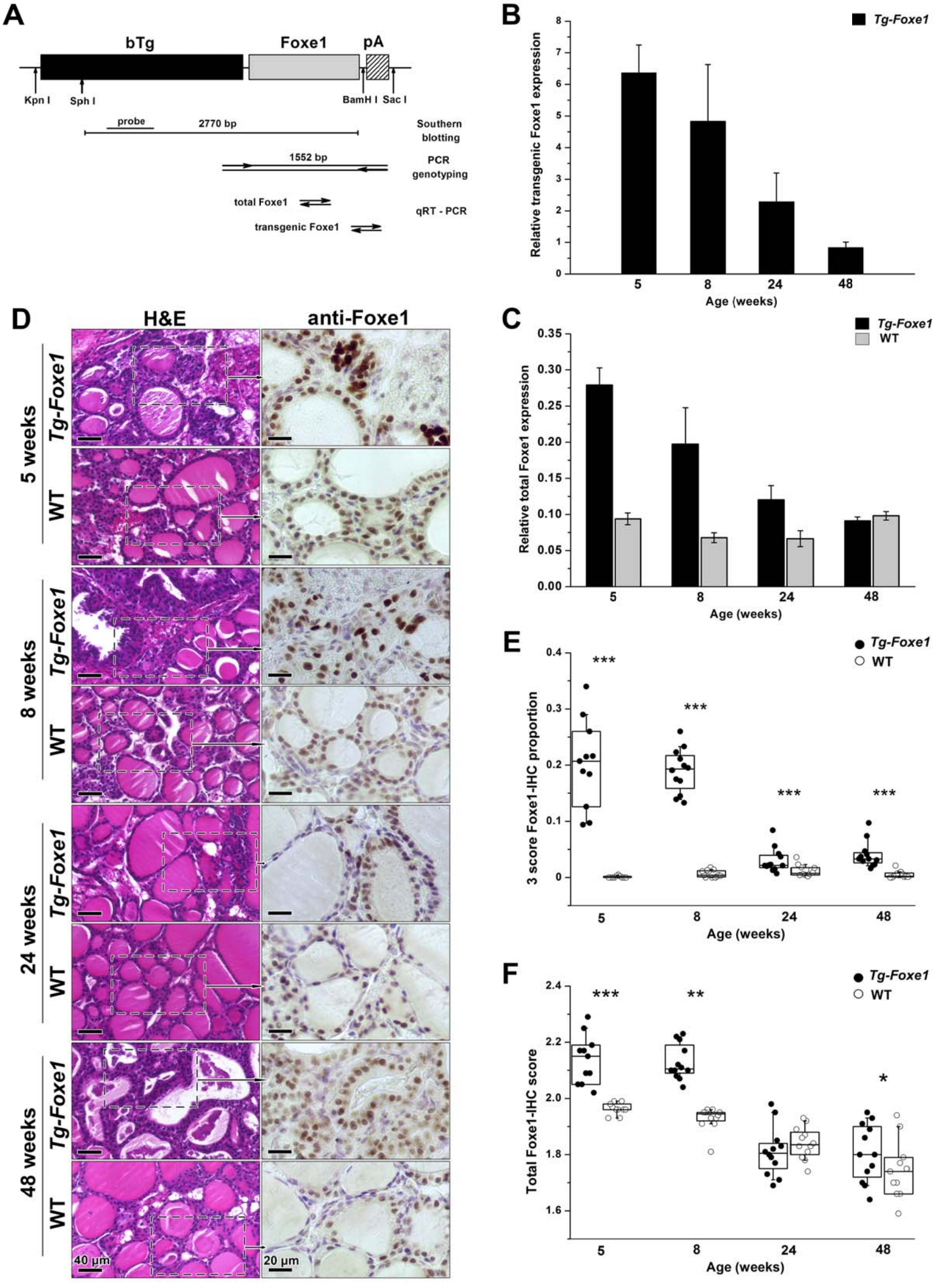
A
bTg
Foxe1
pA
Kpn I
Sph I
BamH I
Sac I
probe
2770 bp
Southern blotting
1552 bp
PCR genotyping
total Foxe1
transgenic Foxe1
qRT - PCR
B
Tg-Foxe1
Relative transgenic Foxe1 expression
Age (weeks)
C
Tg-Foxe1
WT
Relative total Foxe1 expression
Age (weeks)
D
H&E
anti-Foxe1
5 weeks
8 weeks
24 weeks
48 weeks
Tg-Foxe1
WT
40 μm
20 μm
E
Tg-Foxe1
WT
3 score Foxe1-IHC proportion
Age (weeks)
F
Tg-Foxe1
WT
Total Foxe1-IHC score
Age (weeks)

Figure 2

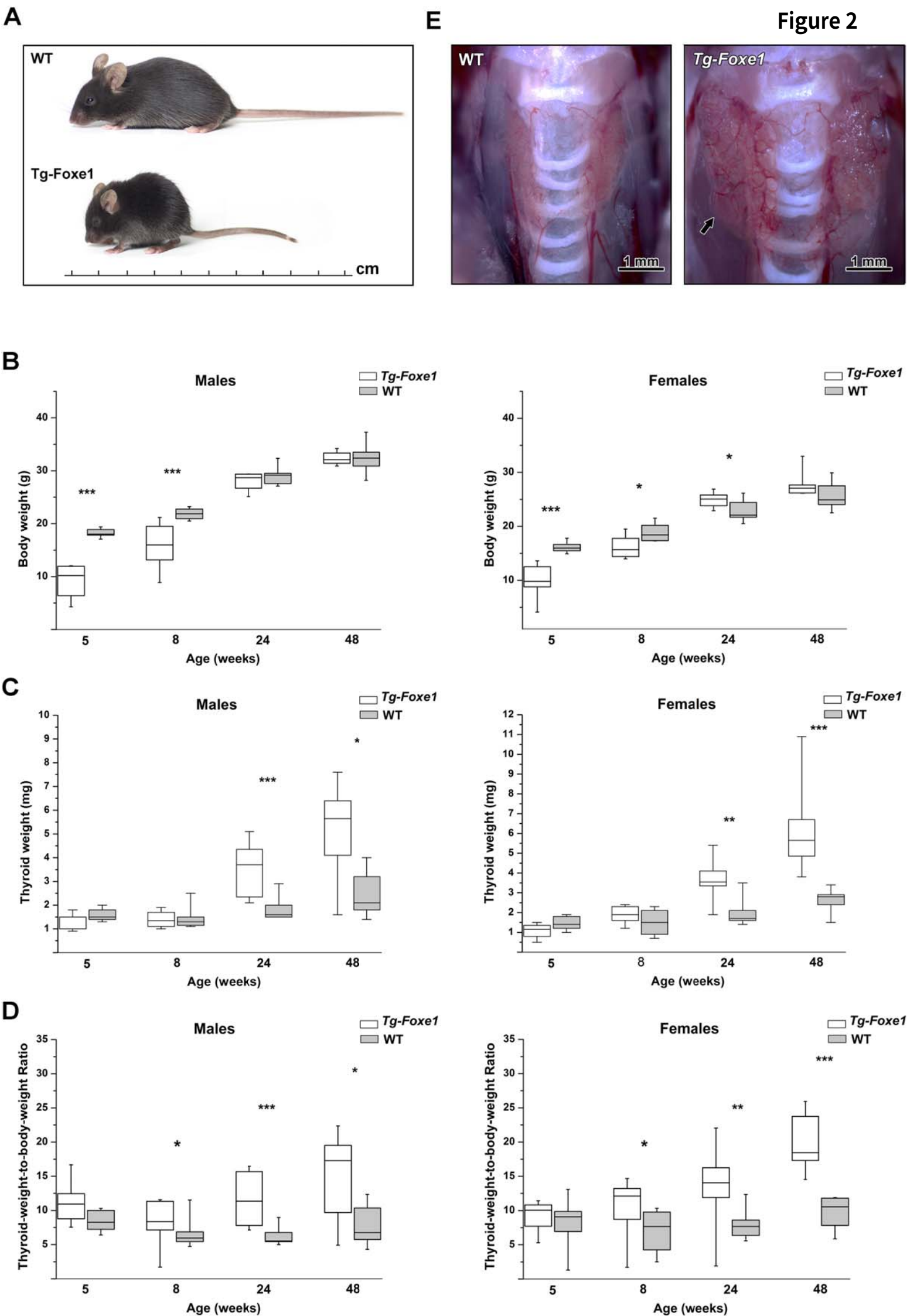
A
WT
Tg-Foxe1
cm
E
WT
Tg-Foxe1
1 mm
1 mm
B
Males
Females
Tg-Foxe1
WT
Body weight (g)
Age (weeks)
C
Thyroid weight (mg)
D
Thyroid-weight-to-body-weight Ratio

Figure 3

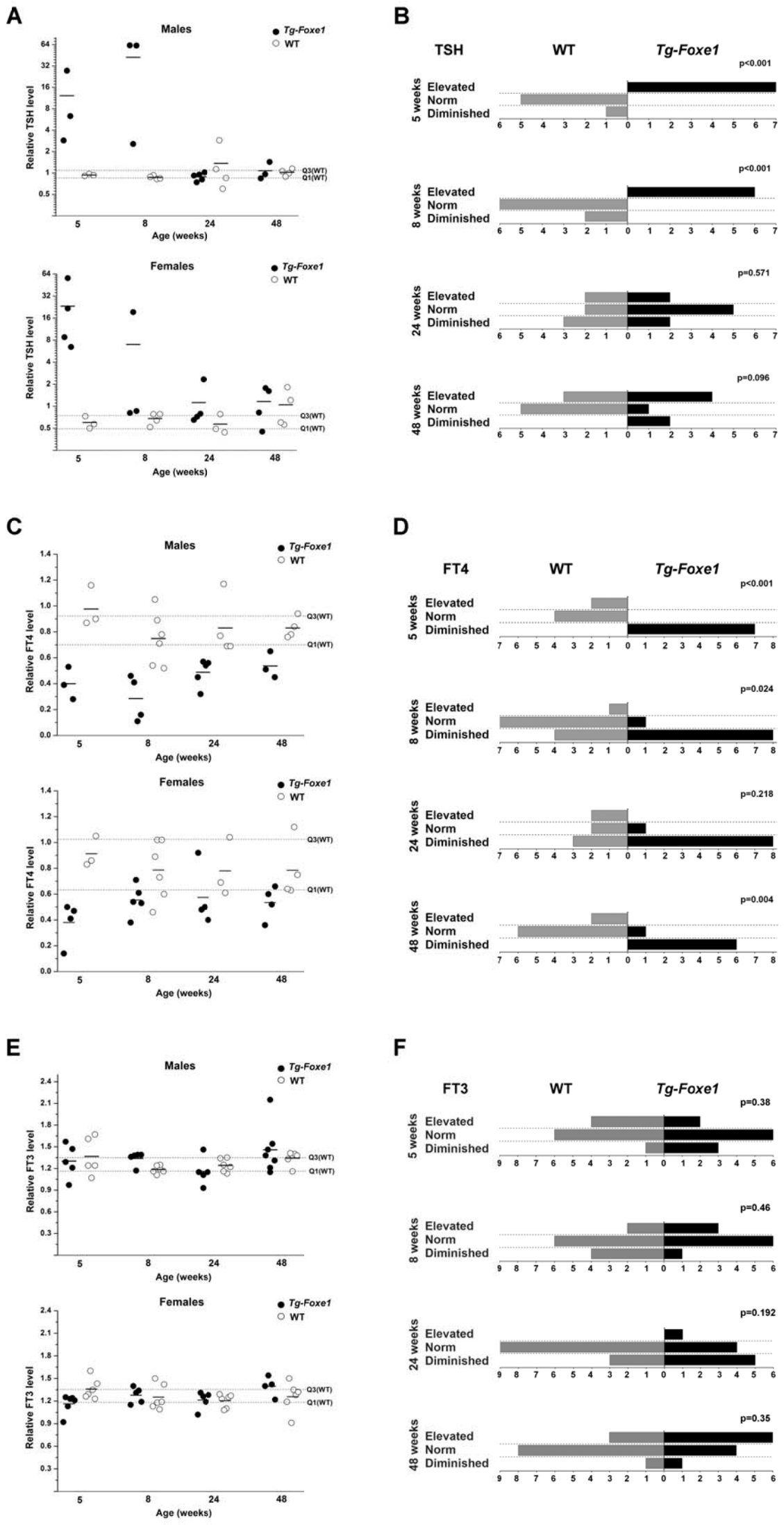
A
Males
Tg-Foxe1
WT
Relative TSH level
Q3(WT)
Q1(WT)
Age (weeks)
Females
B
TSH
WT
Tg-Foxe1
5 weeks
8 weeks
24 weeks
48 weeks
Elevated
Norm
Diminished
p<0.001
p<0.001
p=0.571
p=0.096
C
Relative FT4 level
D
FT4
p<0.001
p=0.024
p=0.218
p=0.004
E
Relative FT3 level
F
FT3
p=0.38
p=0.46
p=0.192
p=0.35

Figure 4

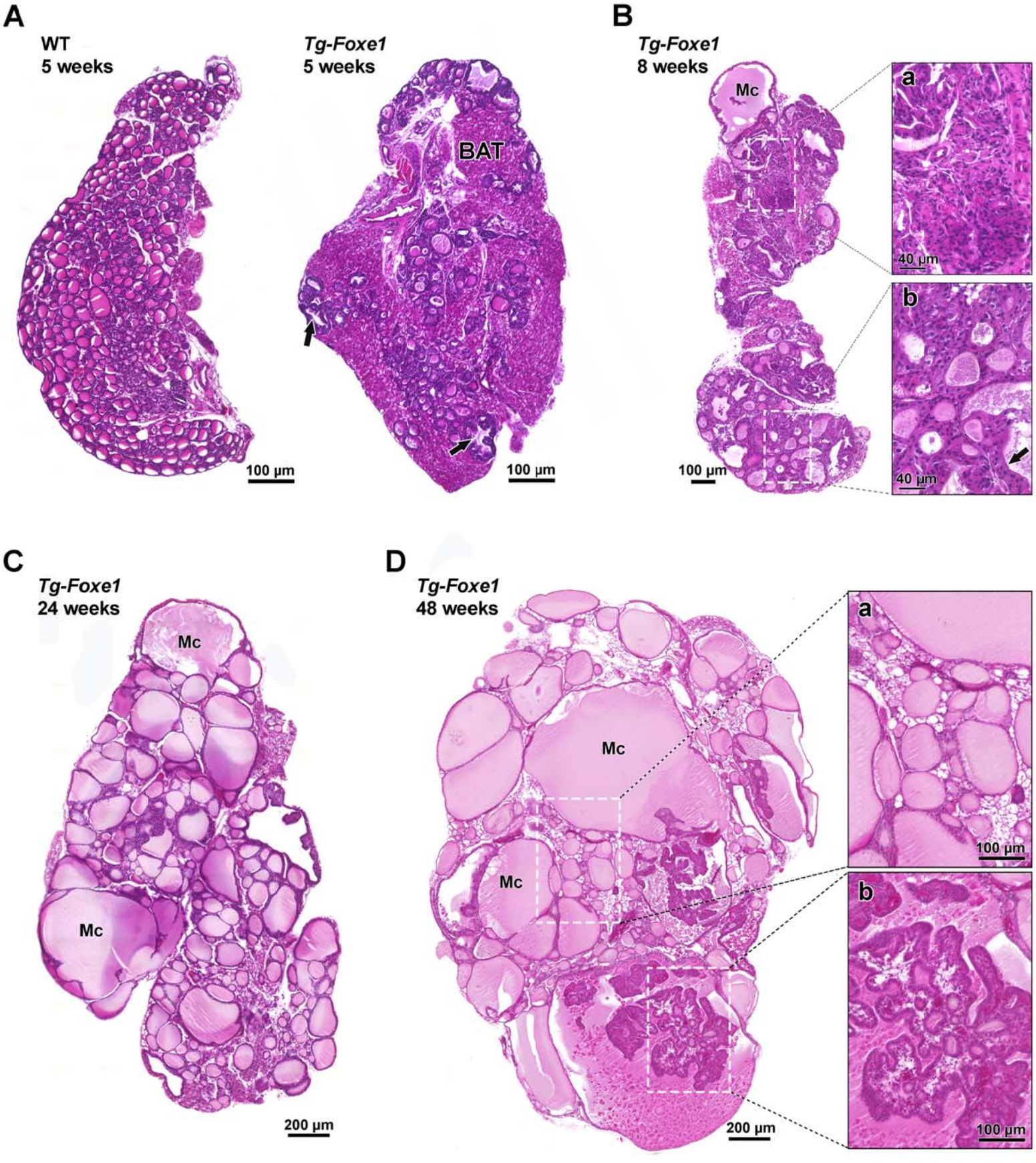
A
WT
5 weeks
100 µm
Tg-Foxe1
5 weeks
BAT
100 µm
B
Tg-Foxe1
8 weeks
Mc
100 µm
a
40 µm
b
40 µm
C
Tg-Foxe1
24 weeks
Mc
Mc
200 µm
D
Tg-Foxe1
48 weeks
Mc
Mc
200 µm
a
100 µm
b
100 µm

Figure 5

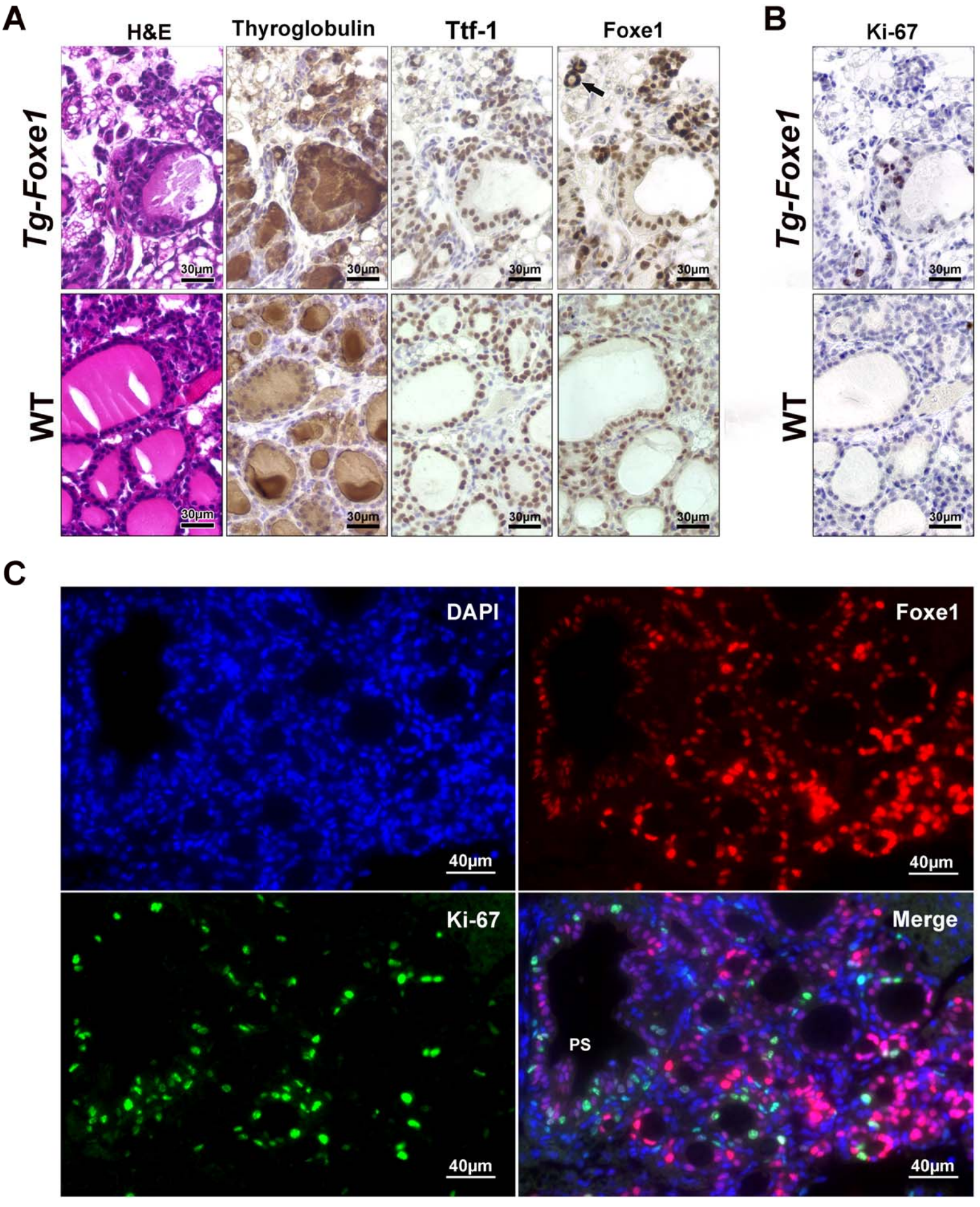
A
H&E
Thyroglobulin
Ttf-1
Foxe1
Tg-Foxe1
WT
30μm
B
Ki-67
Tg-Foxe1
WT
30μm
C
DAPI
Foxe1
Ki-67
Merge
PS
40μm

Figure 6

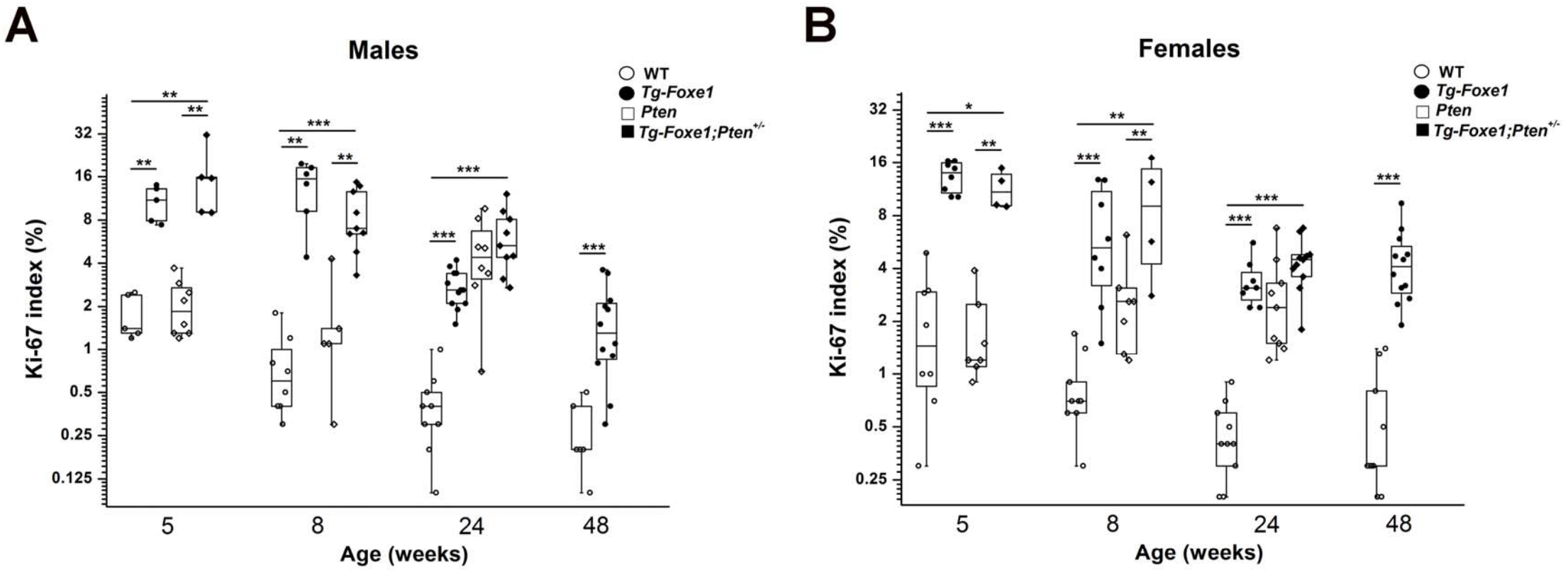
A
Males
WT
Tg-Foxe1
Pten
Tg-Foxe1;Pten+/-
Ki-67 index (%)
32
16
8
4
2
1
0.5
0.25
0.125
5
8
24
48
Age (weeks)
B
Females
WT
Tg-Foxe1
Pten
Tg-Foxe1;Pten+/-
Ki-67 index (%)
32
16
8
4
2
1
0.5
0.25
5
8
24
48
Age (weeks)

Figure 7

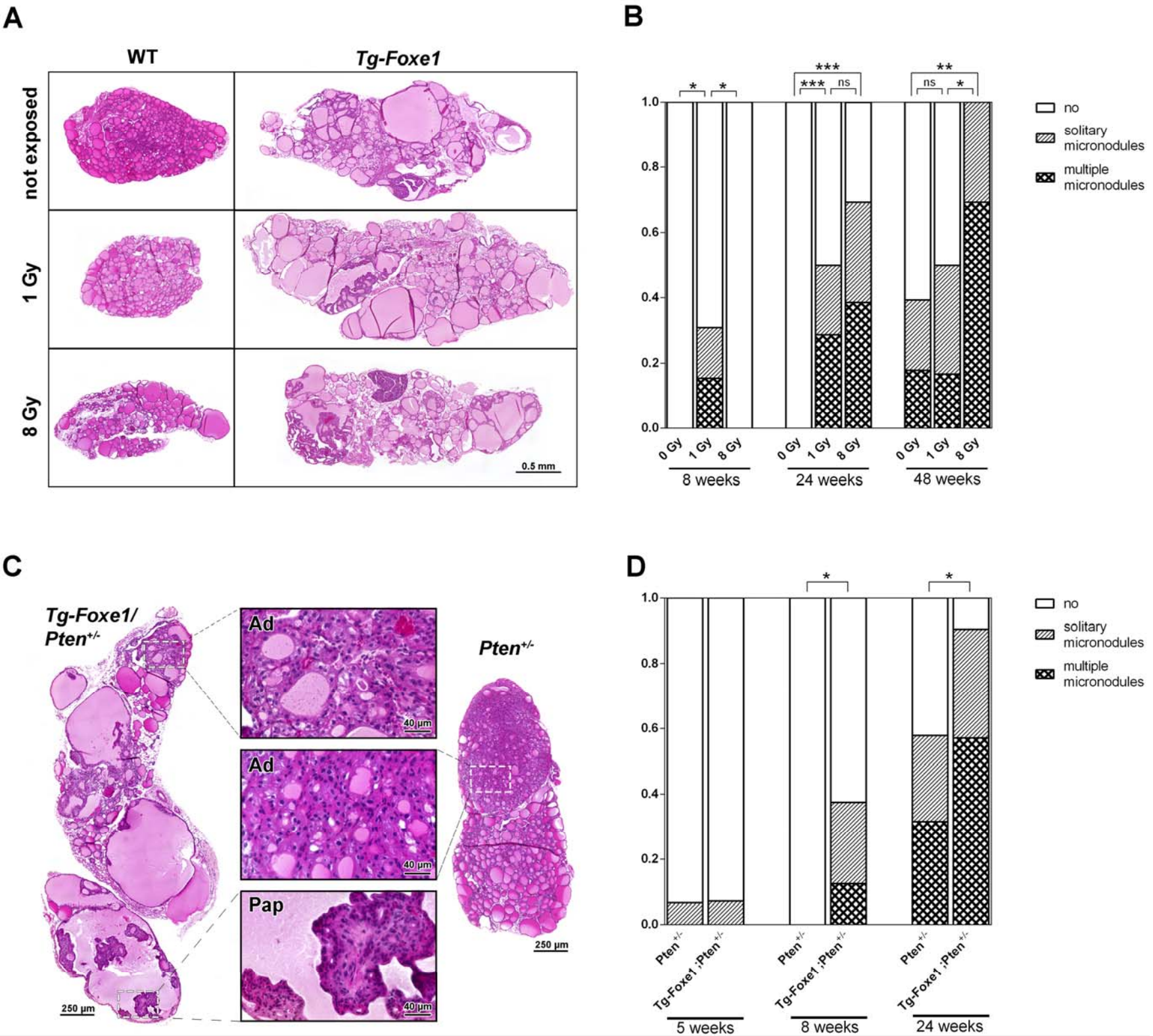
A
WT
Tg-Foxe1
not exposed
1 Gy
8 Gy
0.5 mm
B
no
solitary micronodules
multiple micronodules
0 Gy
1 Gy
8 Gy
8 weeks
24 weeks
48 weeks
C
Tg-Foxe1/ Pten+/-
Pten+/-
Ad
Ad
Pap
40 µm
250 µm
D
Pten+/-
Tg-Foxe1 ;Pten+/-
5 weeks
8 weeks
24 weeks

Supplemental Figure 1

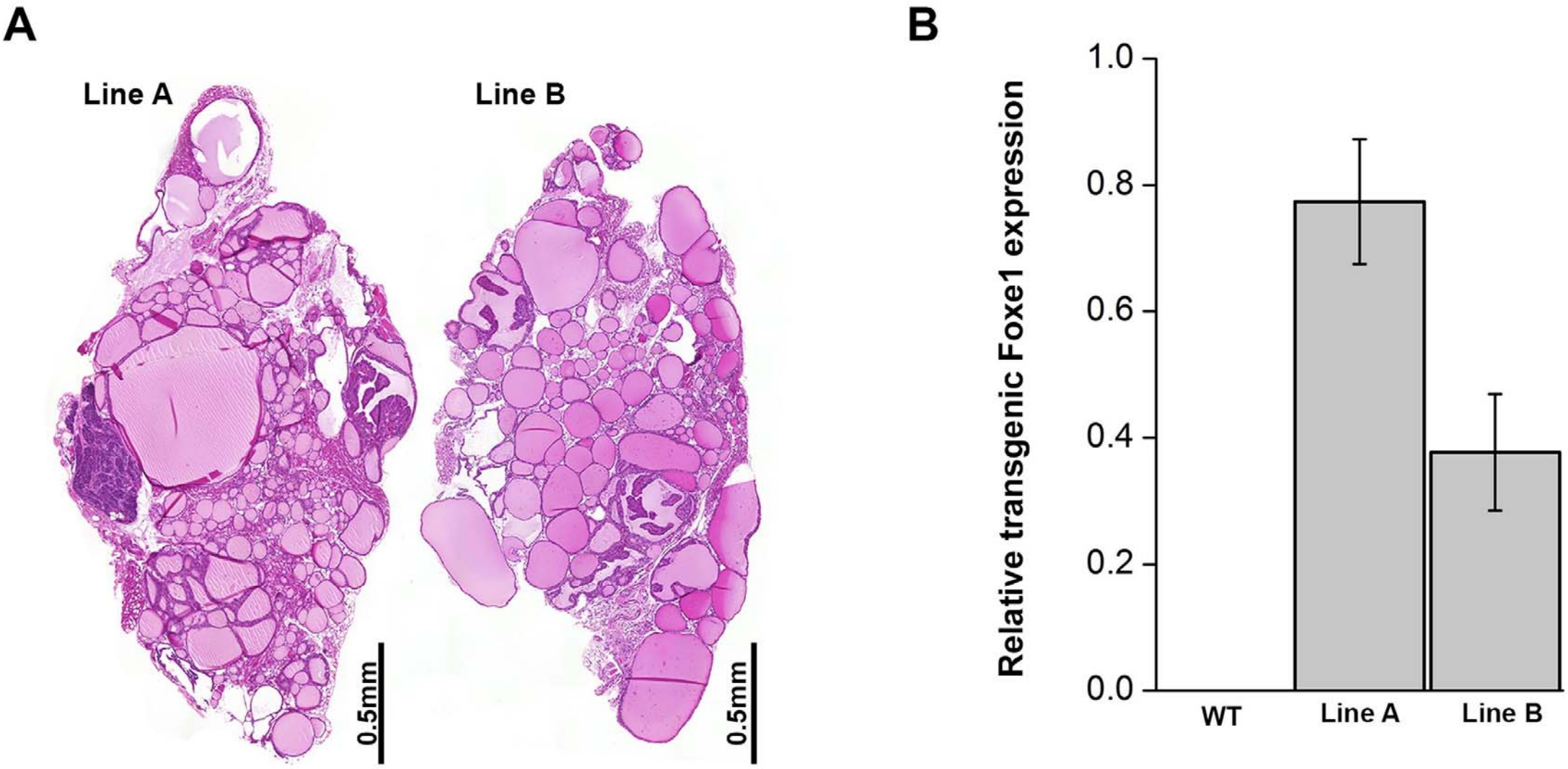

Supplemental Figure 2

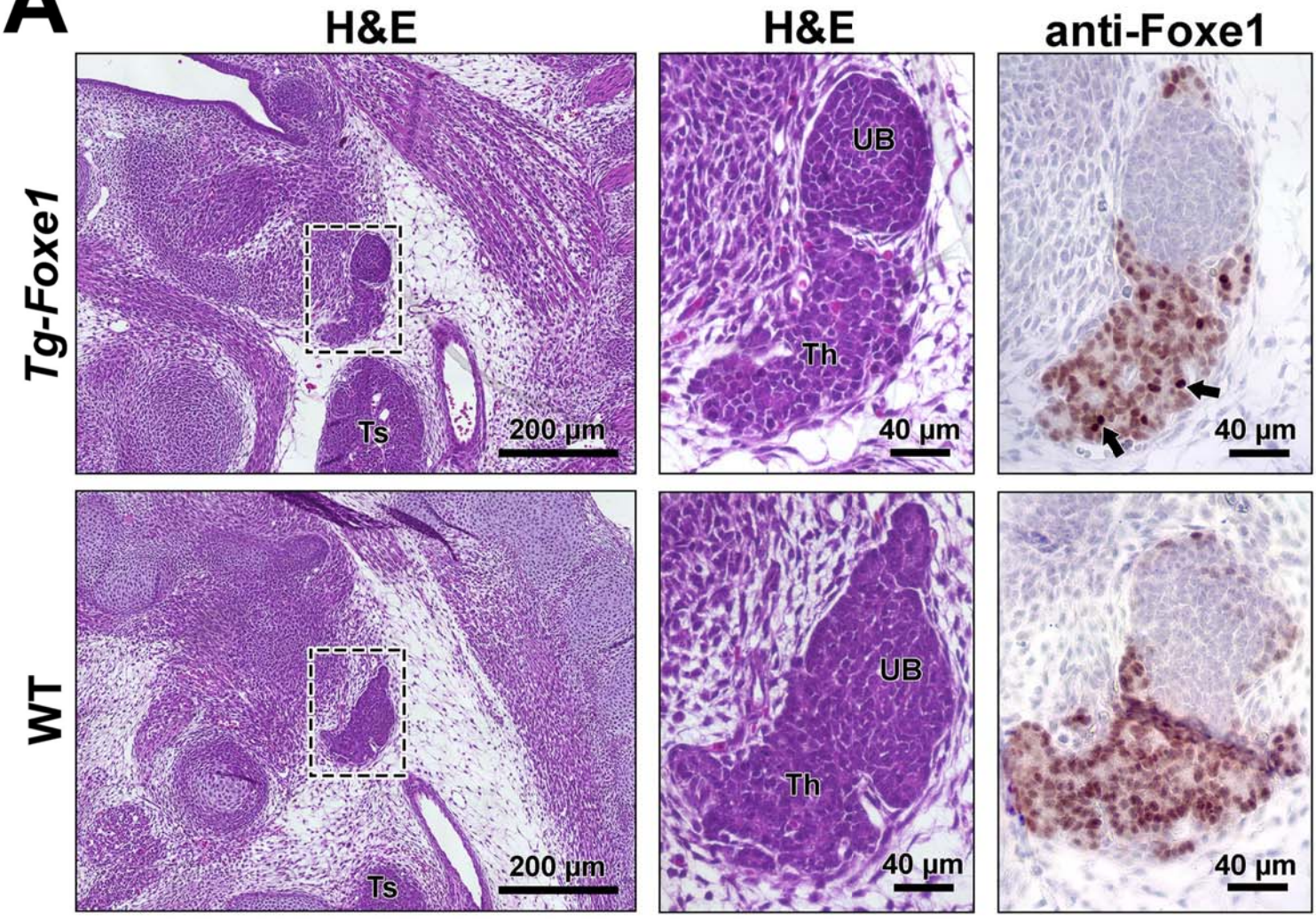

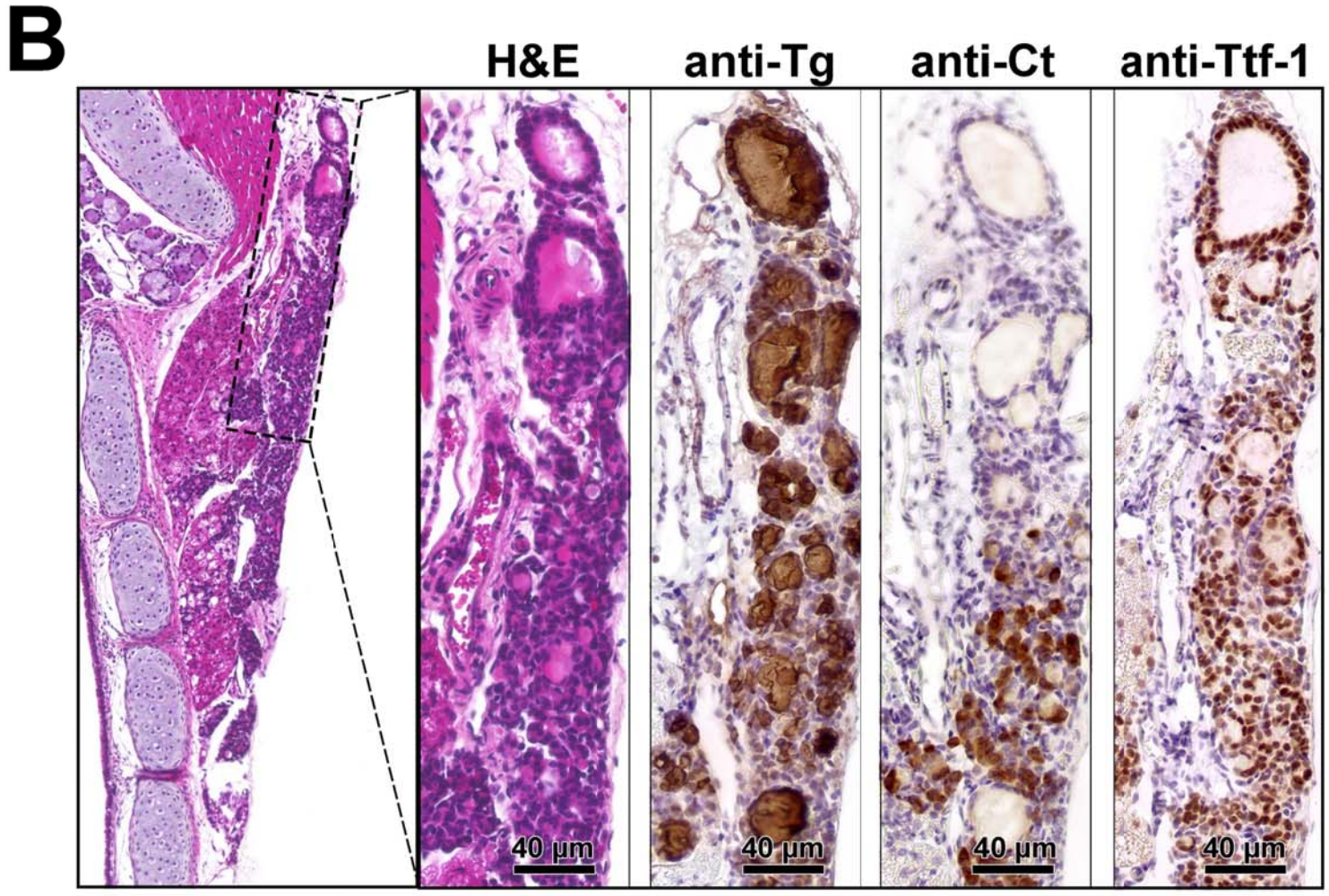

Supplemental Figure 3

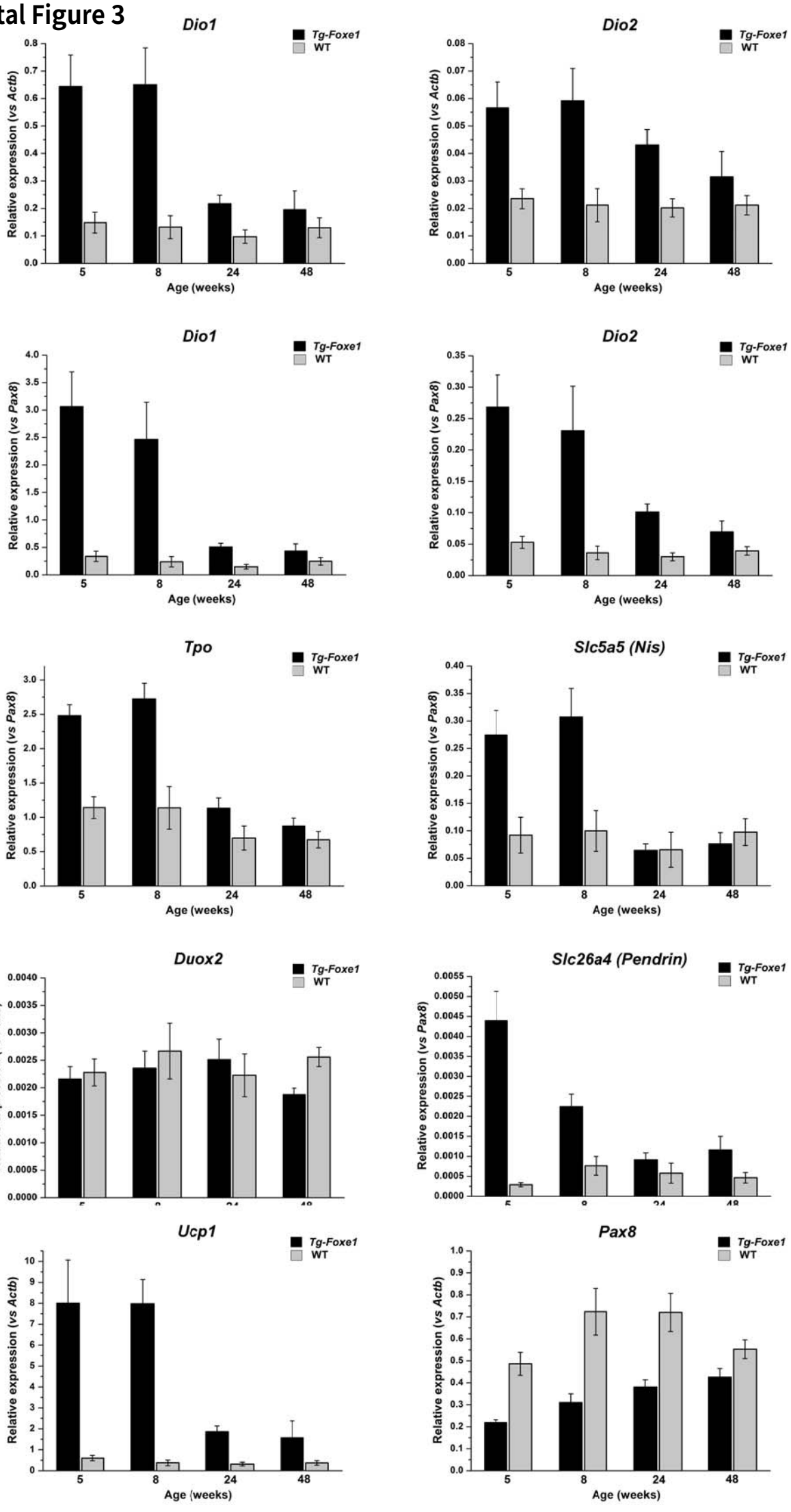

Supplemental Figure 4

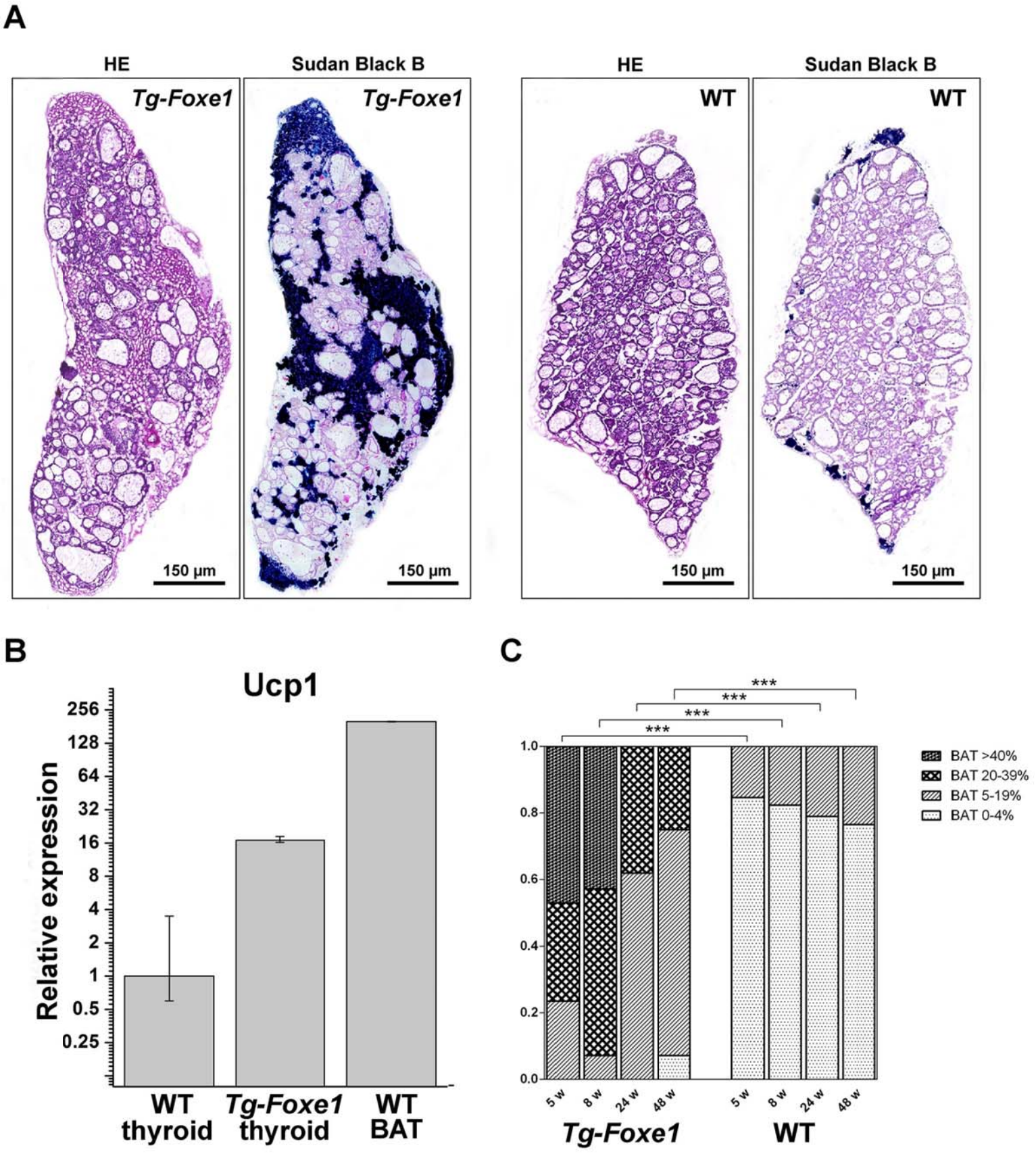

Supplemental Figure 5

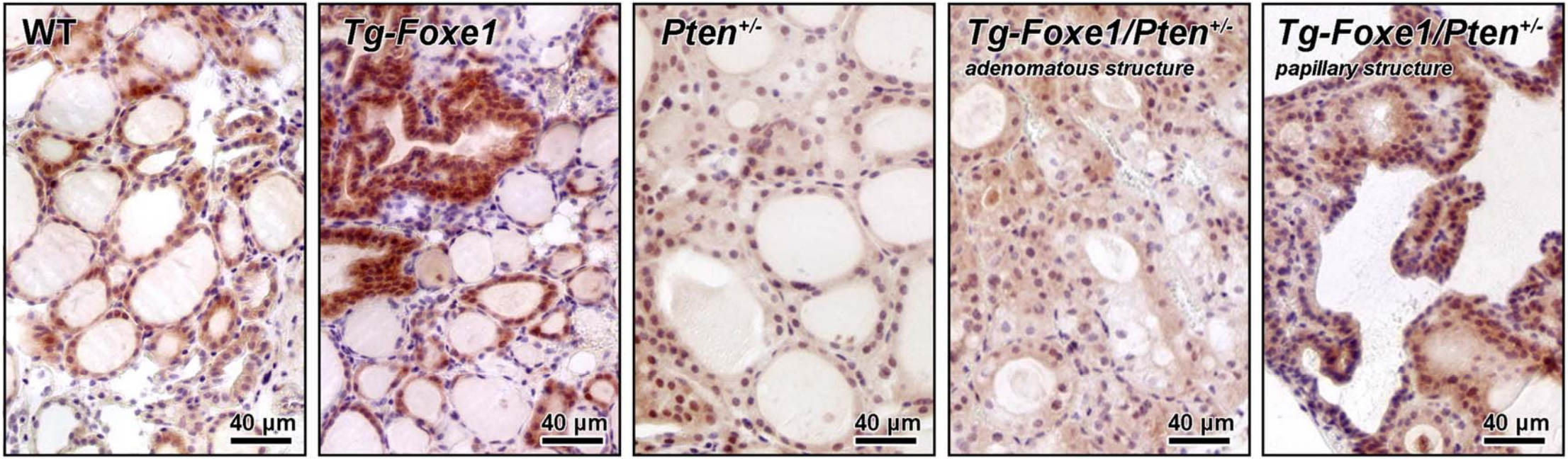

Supplemental Table 1

Peptide/protein target	Antigen sequence (if known)	Name of Antibody	Manufacturer, catalog #, and/or name of individual providing the antibody	Species raised in; monoclonal or polyclonal	Dilution used
TTF-1	-	anti-TTF1	Biopat, Italy, cat.no. PA 0100	rabbit; polyclonal	750
FOXE1 (TTF2)	-	anti-TTF2	Biopat, Italy, cat.no. PA 0200	rabbit; polyclonal	750
Thyroglobulin	-	anti-Human Thyroglobulin	Dako, Denmark, cat.no. A 0251	rabbit; polyclonal	1000
Ki-67	-	anti-Mouse Ki67 Antigen	Dako, Denmark, cat.no. M7249	rat; monoclonal	100
PTEN		anti-PTEN	Abcam, UK, cat. no. ab31392	rabbit; polyclonal	400
Calcitonin	-	anti-Human Primary Calcitonin	Dako, USA, cat.no. IR 515	rabbit; polyclonal	prediluted
Rat Immunoglobulins	-	Anti-Rat Immunoglobulins/HRP	Dako, Denmark, cat.no. P0450	rabbit; polyclonal	100
Rabbit Immunoglobulins	-	Anti-Rab. Immunoglobulins/HRP	Dako, Denmark, cat.no. P0448	goat; polyclonal	100
Rat Immunoglobulins	-	Alexa Fluor 647	Invitrogen, USA, A21247	goat; polyclonal	1000

Supplemental Table 2

Gene	Forward (5'-3')	Reverse (5'-3')	Amplicon size, bp	Reference
transgenic *Foxe1*	CTGCCATGTGAGGATCC	TCATTTTATGTTTCAGGTTCAGG	264	this work
total *Foxe1*	AACCTCACCCTCAACGACTG	GCTTTCGAACATGTCCTCGG	108	this work
Tpo	TGACTTCCAGGAGCACACAG	GCAAGTTCAGTGATGCCAGA	224	Supplemental ref. 1
Slc5a5 (Nis)	GCTCAGTCTCGCTCAAAACC	CGTGTGACAGGCCACATAAC	166	Supplemental ref. 1
Duox2	GGACAGCATGCTTCCAACAAGT	GCCTGATAAACACCGTCAGCA	223	Supplemental ref. 1
Slc26a4 (Pendrin)	CTGAACAGGTACTGCTGCCA	TCAAGGAATGGCTCCTCAGT	104	https://mouseprimerdepot.nci.nih.gov/
Ucp1	AGGTGTGGCAGTGTTCATTGG	TGTAAGCATTGTAGGTCCCCG	113	this work
Pax8	GGCAGAACCCTACCATGTTTG	TCTGTTGATGGAGCTGACACTG	101	this work
Actb (β-actin)	CTGAACCCTAAGGCCAACCGTG	GGCATACAGGGACAGCACAGCC	101	Supplemental ref. 1
Dio1	GCAACTGCCAAAGTTCAACA	GGAAGACAGGGCTGAGTTTG	127	https://mouseprimerdepot.nci.nih.gov/
Dio2	ATTCAGGATTGGAGACGTGC	ATGCTGACCTCAGAAGGGC	121	https://mouseprimerdepot.nci.nih.gov/

Supplemental reference

1. Knauf JA, Ma X, Smith EP, Zhang L, Mitsutake N, Liao XH, Refetoff S, Nikiforov YE, Fagin JA. Targeted expression of BRAFV600E in thyroid cells of transgenic mice results in papillary thyroid cancers that undergo dedifferentiation. Cancer Res 2005; 65:4238-4245.